LBL-23391 c.2

Lawrence Berkeley Laboratory
UNIVERSITY OF CALIFORNIA

Materials & Chemical Sciences Division

RECEIVED
LAWRENCE
BERKELEY LABORATORY

JAN 8 1988

LIBRARY AND
DOCUMENTS SECTION

Laser-Induced Vaporization of Uranium Dioxide

S.K. Yagnik and D.R. Olander

October 1987

LBL-23391 c.2

Prepared for the U.S. Department of Energy under Contract DE-AC03-76SF00098

DISCLAIMER

This document was prepared as an account of work sponsored by the United States Government. While this document is believed to contain correct information, neither the United States Government nor any agency thereof, nor the Regents of the University of California, nor any of their employees, makes any warranty, express or implied, or assumes any legal responsibility for the accuracy, completeness, or usefulness of any information, apparatus, product, or process disclosed, or represents that its use would not infringe privately owned rights. Reference herein to any specific commercial product, process, or service by its trade name, trademark, manufacturer, or otherwise, does not necessarily constitute or imply its endorsement, recommendation, or favoring by the United States Government or any agency thereof, or the Regents of the University of California. The views and opinions of authors expressed herein do not necessarily state or reflect those of the United States Government or any agency thereof or the Regents of the University of California.

LASER-INDUCED VAPORIZATION OF URANIUM DIOXIDE

S. K. YAGNIK and D. R. OLANDER

Department of Nuclear Engineering,
University of California, and
Materials and Chemical Sciences Division,
Lawrence Berkeley Laboratory,
Berkeley, CA 94720

This work was supported by the U.S. Department of Energy
under Contract Number DE-AC03-76SF00098.

Table of Contents

TABLE OF CONTENTS i
LIST OF FIGURES iii
ABSTRACT vi
INTRODUCTION 1
REVIEW OF PAST WORK 4
1 CALIBRATION OF MASS SPECTROMETER 4
2 LASER-DRIVEN VAPORIZATION 6
2.1 Free-Molecule Flow 7
2.2 Collision-Dominated flow 8
3 PRINCIPAL RESULTS 9
4 POSSIBLE SOURCES OF THE DISCREPANCY 10
4.1 Temperature Measurement 10
4.2 Signal Corrections 11
4.3 Collimator Efficiency 11
4.4 Mass spectrometer Saturation or Malfunction 11
4.5 Validity of Theoretical Models 12
EXPERIMENTAL 13
1 LASER SYSTEM 13
1.1 Temporal Pulse Shape 13
1.2 Spatial Intensity Distribution 15
1.3 Laser Irradiance 19
2 DATA COLLECTION 20
THE TEMPERATURE MEASUREMENT 22
1 DESCRIPTION OF THE OPTICAL PYROMETER 22
2 AVOIDANCE OF WINDOW COATING 22
3 PYROMETER CALIBRATION 23
4 VALIDATION OF MEASURED TEMPERATURES 26
4.1 Comparision of Measured and Computed Temperatures 26
4.2 Luminosity of Vapor Plume 34
THE MASS SPECTROMETER RESPONSE 37
1 MASS SPECTROMETER MALFUNCTION 39
1.1 Nitrogen Doser Test 39
1.2 Stability opf Controller Settings 43
2 COLLIMATOR EFFICIENCY 44
RESULTS 50
1 MASS SPECTROMETER CALIBRATION 50

1.1 Stoichiometric Specimens 50
1.2 Hypostoichiometric Specimens 53
2 MASS SPECTROMETER SIGNALS 55
2.1 Temporal Shape 55
2.2 Signal Magnitude 60
2.3 Comparison with Ref [1] 62
3 IONIZATION OF EMITTED VAPOR 62
3.1 Low Laser Irradiance 62
3.2 Thermodynamic State of the Vapor 63
3.3 Ion Detection and Deflection 63
4 TARGETS OTHER THAN UO_2 66
5 SURFACE HEATING RATES 68
3 NEUTRON ACTIVATION ANALYSIS 70
DISCUSSION 77
1 BACKGROUND 77
2 INTERPRETATIONS 78
2.1 Validity of Free-Molecule Flow 78
2.2 Condensation of Vapor Blow-Off 78
3 CONCLUSIONS 80
REFERENCES 82

LIST OF FIGURES

Figure 2.1 : Schematics of the Experimental Set-Up

Figure 3.1 : Temporal Shape of the Laser Pulse

Figure 3.2 : Photodiode Tube Calibration

Figure 3.3 : Laser Pulse Energy Calibration, Ref [10]

Figure 3.4 : Comparison of Signals With and Without the Preamplifier, (a) Mass Spectrometer (b) Pyrometer

Figure 4.1 : Schematic Diagram of the Carousel for Avoidance of Pyrometer View-Port Coating

Figure 4.2 : Pyrometer Calibration - "Automatic" Mode

Figure 4.3 : Pyrometer Calibration - "Transient" Mode, Range 1

Figure 4.4 : Pyrometer Calibration - "Transient" Mode, Range 2

Figure 4.5 : Pyrometer Calibration - "Transient" Mode, Range 3

Figure 4.6 : Comparison of Measured and Computed Surface Temperature Histories of a Typical Laser Shot.

Figure 4.7 : Photomicrograph of UO_2 Target Surface Irradiated with a pulse of $QP = 6.4 \times 10^4$ W/ cm^2. $T_{smax} = 3676K$ measured; $T_{smax} = 3648K$ computed.

Figure 4.8 : The Measured Response of the Pyrometer sighted on locations marked.

Figure 5.1 : Mass Spectrometer Controller Setting Calibration

Figure 5.2 : Schematics of the Experimental Set-up used for the Nitrogen Doser Tests

Figure 5.3 : Mass Spectrometer Signal as a Function of P_{eq} , parametric in Electron-multiplier High Voltage Setting.

Figure 5.4 : Mass Spectrometer Signal as a Function of P_{eq} , parametric in Ionizer Emission Current Setting.

Figure 5.5 : Target- Collimator- Detector Geometry

Figure 5.6 : Mass Spectrometer Signal as a Function of Temperature of Masked Chromium Specimens for Collimator Efficiency Determination.

Figure 5.7 : Experimental Collimator Efficiency compared to the assumption of Ref [1] and [2].

Figure 6.1 : Steady State Calibration Data

Figure 6.2 : Comparison of Mass Spectrometer Signal for Various Uranium-bearing Species (Stoichiometric UO_2)

Figure 6.3 : Comparison of Mass Spectrometer Signal for Various Uranium-bearing Species ($UO_{1.96}$)

Figure 6.4 : Comparison of Mass Spectrometer Signal with the Theoretical Calculations of the Number Density, For T_{smax} = 2059 K.

Figure 6.5 : Comparison of Mass Spectrometer Signal with the Theoretical Calculations of the Number Density, For T_{smax} = 2235 K.

Figure 6.6 : Comparison of Mass Spectrometer Signal with the Theoretical Calculations of the Number Density, For T_{smax} = 2430 K.

Figure 6.7 : Comparison of Mass Spectrometer Signal with the Theoretical Calculations of the Number Density, For T_{smax} = 2435 K.

Figure 6.8 : Comparison of Mass Spectrometer Signal with the Theoretical Calculations of the Number Density, For T_{smax} = 2974 K.

Figure 6.9 : Comparison of Mass Spectrometer Signal with the Theoretical Calculations of the Number Density, For T_{smax} = 3403 K.

Figure 6.10 : Mass Spectrometer signal for UO_2^+ plotted against several measured and computed parameters.

Figure 6.11 : Schematics of Ion-Deflecting Electric and Magnetic fields.

Figure 6.12 : Steady State Calibration and Laser Pulsing data for Chromium Target plotted against measured QP and other calculated parameters.

Figure 6.13 : A Comparison of Mass Spectrometer Response for Chromium and ZrO_2

Figure 6.14 : The Target-Collector Geometry for Neutron Activation Analyses

Figure 6.15 : The Amount of Uranium collected as determined by Neutron Activation Analyses as a function of T_{smax}

Figure 6.16 : Scanning Electron Micrograph of an Unpolished UO_2 Target Surface showing Laser Irradiated and Unirradiated Surface Regions.

LASER-INDUCED VAPORIZATION OF URANIUM DIOXIDE

S. K. YAGNIK and D. R. OLANDER

Department of Nuclear Engineering,
University of California, and
Materials and Chemical Sciences Division,
Lawrence Berkeley Laboratory,
Berkeley, CA 94720

ABSTRACT

The vaporization of UO_2 is studied in an experiment utilizing a Nd-glass laser as a millisecond pulsed heat source. The target of solid is held in vacuum and can be rapidly heated to peak temperatures of 4500 K, as measured by a fast response automatic optical pyrometer. The pulse of vapor species from the laser-heated target is detected in-flight by a quadrupole mass spectrometer. This experimental technique was used in past to measure high temperature vapor pressures of nuclear fuel materials UO_2 [1] and UC [2]. The measured vapor pressures were found to be two orders of magnitude lower than the predictions based on thermochemical models and were also lower than other reported investigations.

The purpose of the present work was to investigate this discrepancy in the vapor pressure measurement of UO_2 . The experimental set-up was improved to eliminate possible sources of errors in the temperature measurement and in the transmission and collection of transient signals. The possibility of the mass spectrometer malfunction was also investigated.

The results obtained in the present work indicate that below a maximum target surface temperature of about 2500 K, the free molecule expansion of ablated species is valid as evidenced by a good agreement between theoretical calculations and the measured mass spectrometer signals. At higher surface temperatures the mass spectrometer signals show *two* peaks rather than expected single, faster peak as collisions in the gas phase become dominant and increase the average molecular speed. Also, the magnitude of the measured mass spectrometer signals ceases to increase with increasing surface temperatures beyond ~ 2500 K. It was verified that instrument malfunction is not responsible for this "saturation" of the signal. The possibility of formation of dimers and polymers of UO_2 due to condensation in the collision-dominated vapor plume, cooled by vacuum expansion, could best explain the peculiarities of the mass spectrometer signals.

A method independent of mass spectrometric measurements was also employed to determine the amount of UO_2 vaporized. This involved neutron activation analysis of vapors collected on a collector placed parallel to the laser-heated target in the pathway of vapor plume. The results from these experiments are in good agreement with theoretical predictions based on the vapor pressure of UO_2 target surface temperatures above the melting point of the solid. At lower temperatures, the amount of vaporized material is highly sensitive to the stoichiometry of the solid. Based on the neutron activation analysis data, it is concluded that the surface of a nominally stoichiometric UO_2 specimen could indeed be hyperstoichiometric, and, since only few monolayers of UO_2 are expected to vaporize at low temperatures, a *larger* amount is vaporized compared to a case where vaporization from bulk occurs.

CHAPTER 1

INTRODUCTION

The vaporization behavior of refractory materials is important in many technological applications where severe temperature conditions are encountered. For example, the fuel materials in nuclear reactors routinely attain high temperatures in normal operating conditions and may reach temperatures well above melting points under postulated accidents. Similarly external ceramic tiles for space shuttles must be designed to withstand high temperatures that are realized at the time of re-entry into atmosphere.

The high temperature vaporization behavior of nuclear fuel materials has been extensively investigated. The ultimate goal of these experiments was, and still is, to determine vapor pressure of the fuel material at high temperatures for use in safety analyses of postulated reactor accidents.

At a given temperature the vapor pressure governs the rate at which the material vaporizes. At low temperature the vapor pressure can be measured by conventional methods such as Knudsen effusion and transpiration. However, at high temperatures (3200 K and up) the conventional methods fail because of a lack of high-melting crucibles. To circumvent this problem, several transient heating techniques including electron, neutron and laser irradiation have been employed. All these techniques can successfully elevate the temperature of refractory solids to well above 4000 K in milliseconds.

Several alternatives are available to measure the amount of material vaporized at these high temperatures. An in-situ quadrupole mass spectrometer is one such method. It has a distinct advantage of having the capability of identifying the vaporizing species as well as the total amount vaporized. The identity of the vaporizing species may be different from the condensed phase for non-congruently vaporizing compounds. Tsai [1] and Tehranian [2] used laser pulse heating technique and quadrupole mass spectrometry to measure high temperature vapor

pressure of UO_2 and UC, respectively.

Ohse and coworkers [3] used the depth of crater formed by a laser pulse on the target surface to measure the amount of material vaporized and thus deduce the the vapor pressure of the solid. Recently Ohse et. al. [4] have also used quadrupole mass spectrometry for measuring high temperature vapor pressure of UO_2 . Bober et. al. [5] measured recoil momentum of laser irradiated refractory specimen and the momentum carried away by evaporated vapor species flowing as vapor-jet in vacuum to obtain the vapor pressure. A recent Japanese work [6] also employed similar telescopic measurements on a torsion pendulum suspending UO_2 targets irradiated by a giant Ruby laser.

Although there is considerable scatter in the high temperature vapor pressure data of UO_2 in the literature [7], the vapor pressures of UO_2 and UC as deduced by Tsai [1] and Tehranian [2] using the Hertz-Langmuir vaporization formula were generally lower, by as much as two orders of magnitude, compared to other reported values [7].

The purpose of the present investigation was to follow-up Tsai's [1] work on UO_2 vaporization. In particular careful evaluation of the experimental technique was undertaken to determine sources of experimental error which might explain the discrepancy in the measured vapor pressure and the theoretically expected values. System calibration is a major concern in this method. The pyrometer needs to be calibrated well above the range of available standards. Similarly the mass spectrometer has to be calibrated to detect signal equivalent to instantaneous pressures of several tens of millitorrs in the ionizer.

Chapter 2 of this report briefly reviews the technique and the method of analysis used in Ref [1] and [2]. Chapter 3 deals with the characterization of a new laser system which replaced the the one used in the past in our laboratory. The temperature measurements, pyrometer calibration and the interpretation of measured temperature data are described in Chapter 4. In Chapter 5 two important findings which directly affect the level and linearity of mass spectrometric signals are discussed. Chapters 6 and 7 deal with mass spectrometer calibration method and discussion on interpretation of mass spectrometer signals in

terms of vapor pressure of UO_2 . Finally in Chapter 7 conclusions of the present investigation are given.

CHAPTER 2

REVIEW OF PAST WORK

Figure 2.1 schematically shows the experimental set-up used by Tsai [1] and Tehranian [2]. Detailed description of their technique and method of analysis is given in Ref [1] and [2]. Only a brief review will be given here.

Their method involved irradiation of solid samples held in vacuum by a Nd-glass pulsed laser capable of delivering 50 J pulses about half a millisecond wide. Peak target temperatures of 4500 K were attained and were measured by a fast optical automatic pyrometer. The species vaporizing from the irradiated target were detected in-flight by a quadrupole mass spectrometer. Three transient signals, namely the laser power pulse, the target surface temperature , and the mass spectrometer output were recorded by a waveform recorder.

1. CALIBRATION OF MASS SPECTROMETER

The vapor concentration in the ionizer of the mass spectrometer can be theoretically related to the target surface temperature by application of the Hertz-Langmuir equation and the vapor pressure. The vapor pressure data for UO_2 and UC are well established below their melting points. This information was used to calibrate the mass spectrometer, i.e to relate the mass spectrometer signal to a known vapor concentration in the ionizer at low temperatures (up to ~ 2400 K). The calibration was then used to deduce the high temperature (up to ~ 4200 K) vapor pressure from the observed mass spectrometer signals.

The mass spectrometer calibration was done as follows. An electron beam heater was used to heat a UO_2 sample to a steady temperature in vacuum. The vapor thus generated was collimated and directed towards the ionizer of the mass spectrometer as a steady molecular beam. For UC such a beam was generated by a Knudsen cell filled with UC_2 and excess graphite. The source temperature in both cases was measured by an optical pyrometer.

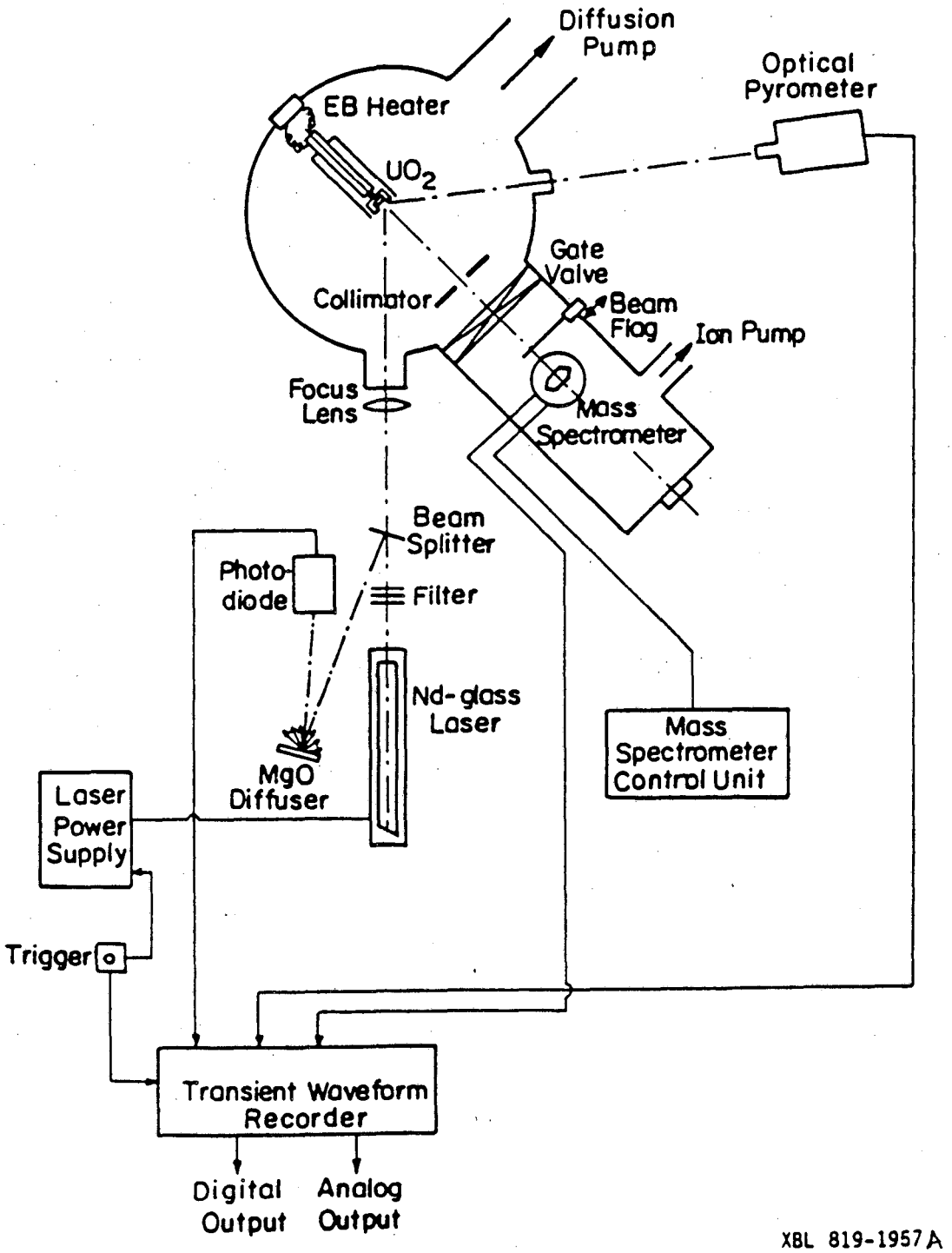
Diffusion Pump
Optical Pyrometer
EB Heater
UO_2
Gate Valve
Collimator
Beam Flag
Ion Pump
Focus Lens
Mass Spectrometer
Beam Splitter
Photo-diode
Filter
Nd-glass Laser
MgO Diffuser
Mass Spectrometer Control Unit
Laser Power Supply
Trigger
Transient Waveform Recorder
Digital Output
Analog Output
XBL 819-1957A

Fig. 2.1

The steady molecular density n in the ionizer at a distance l from the heated source at temperature T is given by

$$n = K_g K_u \frac{P}{T} \tag{2.1}$$

where K_g is the geometric factor, K_u (= 7.32 x 10^{21} molecules-K/ cm^3 -atm)is the unit conversion factor and P is the vapor pressure of the source material at temperature T. The geometric factor K_g is equal to A_s / (4 πl^2), where A_s is the source area viewed by the mass spectrometer. The latter was taken to be the collimator or the Knudsen cell aperture area.

Since UO_2 and UC are incongruently vaporizing solids, steady state signals of UO_2 , UO, U and UO_3 were observed for the UO_2 source and those of UC_2 , U, C_3 and C_1 for the UC source. The mass spectrometer gives a signal S_i proportional to the vapor concentration of species i in the ionizer, namely n_i .

$$S_i = K_{MS}\, \sigma_i\, \gamma_i\, n_i \tag{2.2}$$

where K_{MS} is the instrumental constant (independent of the species being detected), σ_i is the ionization cross-section of neutral species i by 70 volts electrons and γ_i is the average number of secondary electrons generated at the first dynode for each ion collected. The measured signal S_i is further complicated by the fragmentation in the ionizer. The details of fragmentation are considered in Ref [1] and [2] and will be omitted here for simplicity.

By substituting Eq (2.1) into Eq (2.2), ($K_{MS}\, \sigma_i\, \gamma_i$) can be determined from measured calibration signals where the partial pressures P_i are well-established. If the mass spectrometer behaves linearly, the calibration can be used to obtain the vapor pressure at temperatures well above the melting point, attained by firing laser pulses on UO_2 or UC.

2. LASER-DRIVEN VAPORIZATION

The surface temperature transient $T_s(t)$ for the specimen irradiated by the laser pulse was monitored by a fast optical pyrometer. The vapors were collimated and directed towards the ionizer of the mass

spectrometer keeping the same geometry as was used in the calibration. A time dependent output signal was obtained from the mass spectrometer. The transient signals were analytically corrected for the RC delay introduced by the cables and instrumentation. The magnitude of the RC corrected mass spectrometer signal should be proportional to n_i .

Theoretical calculation of $n_i(t)$ depends on the behavior of the laser-driven vapor flow.

2.1. Free-Molecule Flow

The free-molecule model assumes that molecules leaving the target surface do not undergo collisions. The molecules have an angular distribution that varies as $\cos\theta$ and they have a Maxwellian speed distribution. According to this model, the number density in the ionizer from a vaporizing surface with a temperature history $T_s(t)$ is given by

$$n(t) = \frac{\alpha A_s l}{k}\left(\frac{m}{2\pi k}\right)^{3/2}\int_0^t \frac{P[T_s(t)]}{(T_s(t))^{5/2}.(t-\tau)^4}\exp\left[-\frac{ml^2}{2kT_s(t).(t-\tau)^2}\right]d\tau \quad (2.3)$$

where

α = condensation coefficient (assumed = 1)

l= distance between the source and the ionizer (= 40 cm)

A_s= surface area viewed by mass spectrometer (= 7.85×10^{-3} cm^2, based on the collimator opening area)

k= Boltzmann constant

m= mass of the molecule detected

P= vapor pressure of the molecule detected

τ= time of emission of the molecule at the source surface

t= time of arrival of the molecule at ionizer at distance l

Eq (2.3) is based on Hertz-Langmuir vaporization, where the surface rate of vaporization per unit area is given by

$$\phi = \frac{\alpha P(T_s)}{\sqrt{2\pi m k T_s}} \quad (2.4)$$

2.2. Collision-Dominated Flow

As the number density at the target surface increases with increase in T_s , the collisions among the molecules can no longer be ignored. For collision-dominated flow the net rate of vaporization per unit area of the surface is given by

$$\phi = \frac{\alpha P(T_s)(1-\beta)}{\sqrt{2\pi m k T_s}} \tag{2.5}$$

where β is backscattering factor. The molecular angular distribution in this type of flow varies as $\cos^2\theta$,unlike the $\cos\theta$ distribution for free-molecule flow. The speed distribution also becomes modified because of the collisions.

For a surface vaporizing in vacuum, there are three distinct flow regions as described in Ref [2]. First, a collision-dominated Knudsen layer in the immediate vicinity of the surface. This is followed by a hydrodynamic region that eventually turns to a free-molecule flow region as the vapor moves farther away from the surface (Fig 2.11 of Ref [2]).

The mathematical derivation for the number density of the molecules, $n(t)$, at a distance l from the surface for a surface temperature history $T_s(t)$ is given in Appendix C of Ref [2] for the collision-dominated flow model. Briefly, n(t) is the sum of contributions from all molecules whose transit times satisfy the relation :

$$t_{tr}[T_s(\tau)] = t - \tau \tag{2.6}$$

where τ is the time at which molecules leave the surface. The transit time of the molecules to the ionizer of the mass spectrometer is equal to $\frac{l}{u_T}$, where u_T is the terminal velocity of the molecules emitted at surface temperature T_s . The number density n(t) is given by :

$$n(t) = \frac{1}{l^2 F}\left[\frac{\phi(\tau_1)}{u_T(\tau_1)} + \frac{\phi(\tau_2)}{u_T(\tau_2)} + \ldots\ldots\right] \tag{2.7}$$

where $\tau_1, \tau_2, \ldots$ are the roots of Eq (2.6) for time t, and $F = 2\pi\int_0^{\pi/2}$

$f(\theta)d(\cos\theta)$,$f(\theta)$ being the angular distribution.

3. PRINCIPAL RESULTS

By tuning the mass spectrometer to detect different species during the transient heating of the target and using the mass spectrometer calibration as determined by the method given in section 2, Eq (2.3) (or the equivalent equation for the collision-dominated flow) can be deconvoluted to obtain the partial pressures of those species.

The output signals from the mass spectrometer for UO_2 showed two peaks. The first peak was attributed to fast ions that may have been generated intrinsically from the solid target or by the laser interaction on the vapor cloud. The second peak was due to the neutrals. Concluding that the percentage of ionization is low, Tsai [1] ignored the fast peak for his vapor pressure calculations. For UC specimens, however, Tehranian [2] did not observe the fast first peak. He observed mass spectrometer signals containing only one peak.

Another interesting feature of the RC-corrected signals for UO_2 was that the second slower peak occurred later in time compared to the theoretical model predictions based on the free-molecule flow. For UC, where the signals had only peak, the molecules also appeared to be slower compared to the free-molecule flow model. Fig 4.17 of Ref [1] and Fig 4.9 of Ref [2] illustrate this. The delay was nearly 200 μs in the experimentally observed peak value of the number density as compared to the free-molecule flow model. This would mean that the molecules are traveling *slower* than the Maxwellian speed. It remined a puzzling experimental observation.

An attempt was made by Tehranian [2] to account for molecular collisions in the vapor cloud in a gasdynamic model where the three different flow regions described earlier were considered. Calculations based on this model predicted that the molecules tend to speed up because of the collisions. This would mean a shorter time of arrival than predicted by the free-molecule model, not the observed longer time of arrival. The gasdynamic model thus failed to account for the observed delay in signals peaks and the presence of two peaks for UO_2 .

Calculations based on gasdynamic model for the time of the maximum number density are also shown on Fig 4.17 and 4.9 of Ref [1] and [2] respectively for comparision.

The inferred high temperature vapor pressures of UO_2 were nearly two orders of magnitude lower than those predicted by Blackburn's thermochemical model [8]. These values are equally lower compared to those reported by other investigators and compiled * in Ref [7]. For UC [2] the calculated number densities in the ionizer remained virtually unchanged with increase in laser pulse energy between 5.9 to 14.5 J because the magnitude of mass spectrometer signals remained unchanged in that range (Fig 4.11 to 4.13 in Ref [2]). The energy range corresponds to irradiance ranging from 1.6×10^5 to 4.0×10^5 W/ cm^2, and the measured maximum surface temperature ranging from 2910 to 5290 K. Why the mass spectrometer signal remained nearly unchanged over such a large temperature range remained unexplained in Ref [2].

4. POSSIBLE SOURCES OF THE DISCREPANCY

The objective of the present work was to investigate the discrepancies in the measured and predicted vapor pressures in Ref [1] and [2]. This required a careful evaluation of the experimental procedure to remove possible sources of error. The following aspects of the experimental procedure were examined.

4.1. Temperature Measurement

Temperature is a key variable in these measurements. The temperature as measured by the fast optical automatic pyrometer must be reliable. A modified pyrometer calibration procedure was adopted. The long-term drift in the pyrometer and other important aspects of the functioning of the instrument were examined to assign error limits to the

* Although Fig 4.19 of Ref [1] shows a good agreement between the measured vapor pressures and Blackburn's thermochemical model, the measured values are in fact a factor of 100 lower because of a calculational error in the geometric factor K_g in Ref [1].

measured temperature data. The experimental set-up was improved to eliminate measured temperature errors resulting from coating of the pyrometer view port. These details will be discussed in Chapter 4.

4.2. Signal Corrections

The RC corrections of the recorded transient signals were done analytically in Ref [1] and [2] by using manufacturers' suggested numbers for the input resistance and the capacitance of the waveform recorder and the cables. In addition to being tedious, the analytical corrections may be in error owing to its reliance solely on the specifications of the instruments and cables. Further, there is no independent way to ascertain that the corrected transients are indeed accurate. In the present work, therefore, suitable current-to-voltage converting preamplifiers were installed to avoid the need for RC corrections of the recorded transients. This will be discussed further in Chapter 3.

4.3. Collimator Efficiency

The area of the heated target surface viewed by the mass spectrometer, namely term A_s in Eq (2.3), was taken to be equal to the collimator opening area (i.e. 1 mm diameter in Ref [1] and [2]). The validity of using such a value for A_s was never independently confirmed. It was found during this work that the mass spectrometer responds to an area on the target surface much larger than the collimator opening. Chapter 5 will describe the collimator efficiency as applied to the mass spectrometer response, and its experimental determination.

4.4. Mass Spectrometer Saturation or Malfunction

It can be argued that the mass spectrometer itself does not respond linearly to number densities in its ionizer varying over several orders of magnitude. For a typical surface temperature used in the calibration of the instrument, the equivalent pressure of UO_2 in the ionizer (which is proportional to the number density) is several orders of magnitude lower than those predicted for laser pulsing when peak surface temperature is about 4500 K. The calibration of the mass spectrometer can be used for

high surface temperature transients only if it can be established that mass spectrometer remains linear and does not "saturate". This was investigated by monitoring the instrument response as a function of independently-established number densities of a test gas in the ionizer. This will be discussed in Chapter 5.

4.5. Validity of Theoretical Models

The free-molecule flow model is the basic model that assumes no interactions in the laser driven vapor flow. On the other hand, the gas-dynamic model accounts for molecular collisions in the vapor. Since the latter model still does not explain the time of the maximum of the mass spectrometer signal and the presence of two peaks for UO_2 , it is possible that more complex phenomena such as gas phase condensation and gas phase reactions may be occurring. These phenomena are too complex to be modeled analytically. In addition, these complexities would substantially reduce the effectiveness of this technique to measure the vapor pressures accurately.

In the present work careful attention was paid to the fast peak evolution. At what surface temperature does the fast peak first appear for UO_2 ? Why the fast peak is not observed for UC ? Is the fast peak really resulting from ions in the vapor ? These aspects are further discussed in Chapters 6 and 7.

CHAPTER 3

EXPERIMENTAL

The experimental set-up used by Tsai [1] and Tehranian [2] was used in this work with some modifications in the vacuum system and instrumentation. However, a new laser system replaced the one previously used. The changes in the vacuum system regarding the temperature and mass spectrometric measurements will be described in later chapters. The characteristics of the new laser system and the preamplifiers, installed to avoid analytical RC corrections of the measured transients, will be described in this chapter.

1. LASER SYSTEM

A Lasermatrics (Model 936 - G4 - L1) normal pulsed Nd-Glass laser is used as a heat source. The system is capable of delivering up to six 50 J pulses per minute of about 750 μ s duration. It has a 6" long and 0.5" diameter Neodymium doped glass rod with planar front and rear reflectors.

1.1. Temporal Pulse Shape

The laser output as monitored by a KORAD KD-1 photodiode tube (see Fig 2.1) gives the time variation of power of the pulse. Fig 3.1 shows a typical temporal pulse shape. The oscillations riding over the pulse are the relaxation oscillations typical of a multimode pulse laser [9].

The pulse width is about 750 μ s with a maximum increase of 25% as the high voltage applied to the capacitor banks of the laser power supply is increased. The effective pulse width, t_{pul} , is the width of a hypothetical constant power pulse at the maximum power level of the real pulse that has the same total energy as the real pulse. From the area under the time varying power of the pulse such as in Fig 3.1, t_{pul} can be calculated. For most pulses in the present laser system t_{pul} is about 450 μ s.

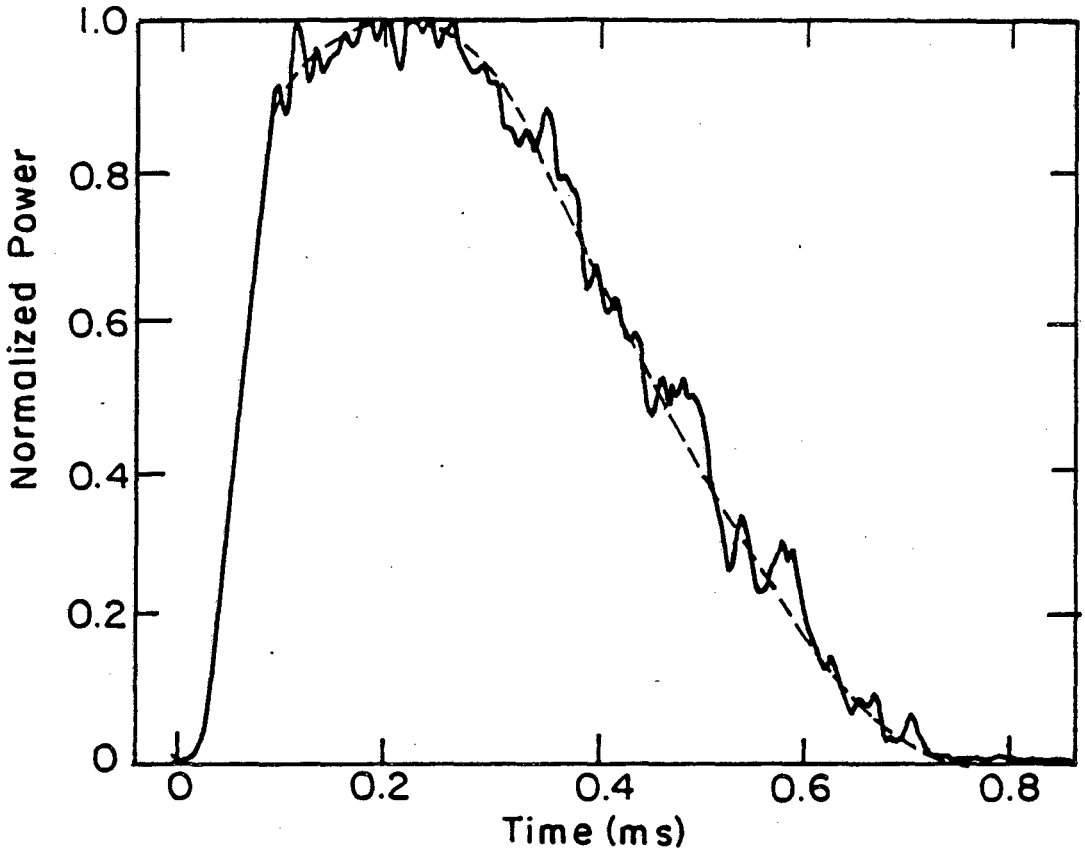

XBL 861-7448A

Fig. 3.1

The total energy contained in a pulse, E, can be obtained using two different approaches. First, the maximum of the signal from the photodiode tube was calibrated against pulse energy measured by a laser calorimeter. This was done in a configuration identical to the one used for the transient heating of the target except for the replacement of the target by a KORAD K-J2 calorimeter. The calibration is shown in Fig 3.2. Components such as lenses, vacuum system windows were kept in place during the calibration to account for their attenuation effects. This way explicit corrections for these components were not necessary. In this method the measured values of beam energy, ultimately depend on the sensitivity factor of the calorimeter (millivolts per Joule) specified by the manufacturer. The sensitivity factor may change over long periods of time because of possible degradation of the calorimeter.

Alternately, the calibration of the laser system specified by the manufacturer [10] can be utilized to infer the value of E for a laser shot. The manufacturer specifies the beam energy as a function of the high voltage setting on the laser power supply as shown in Fig 3.3. This method of deducing beam energy E assumes ideal lasing conditions with precise beam alignment. Also, corrections for the attenuating components have to be made to obtain the energy delivered to the target. This method gives nearly twice the value of E obtained from the former method for most laser shots.

1.2. Spatial Intensity Distribution

A laser pulse has a power distribution in space as well as in time. The spatial energy distribution of the beam is affected by several factors such as the precision of alignment and focus as well as the beam divergence. For a mode-locked laser system whose cavity is resonating in the lowest mode, i.e. TEM_{00}, the spatial intensity distribution becomes Gaussian [9]. However, for a multimode conventional laser system such as the one used in the present work, the spatial energy distribution is far more complex. The spatial distribution in such lasers is known to vary from one shot to other and *within* the duration of a single pulse [9]. The latter characteristics of a multimode laser would generally tend to make time-integrated spatial intensity distribution more uniform.

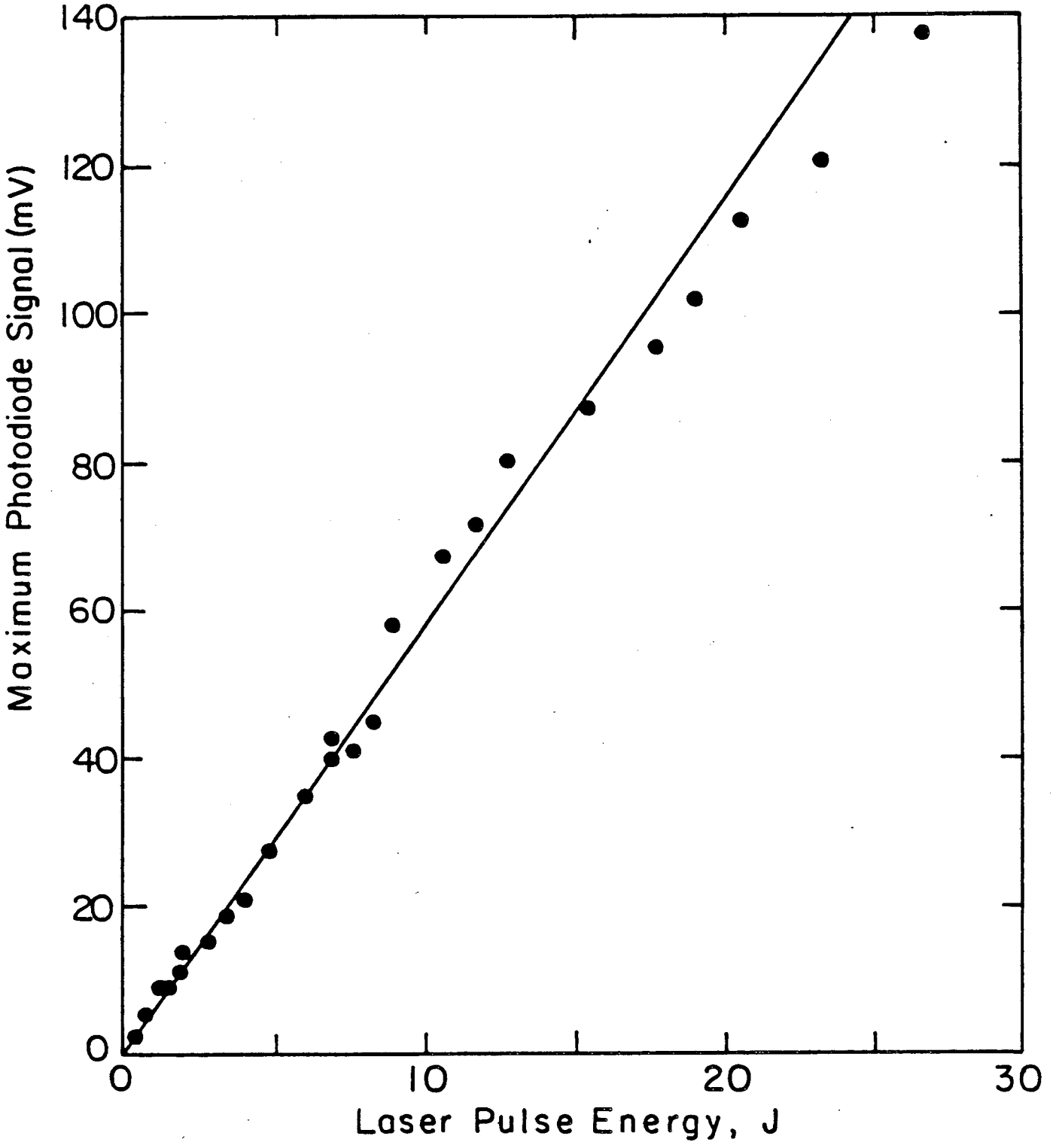

XBL861-7449

Fig. 3.2

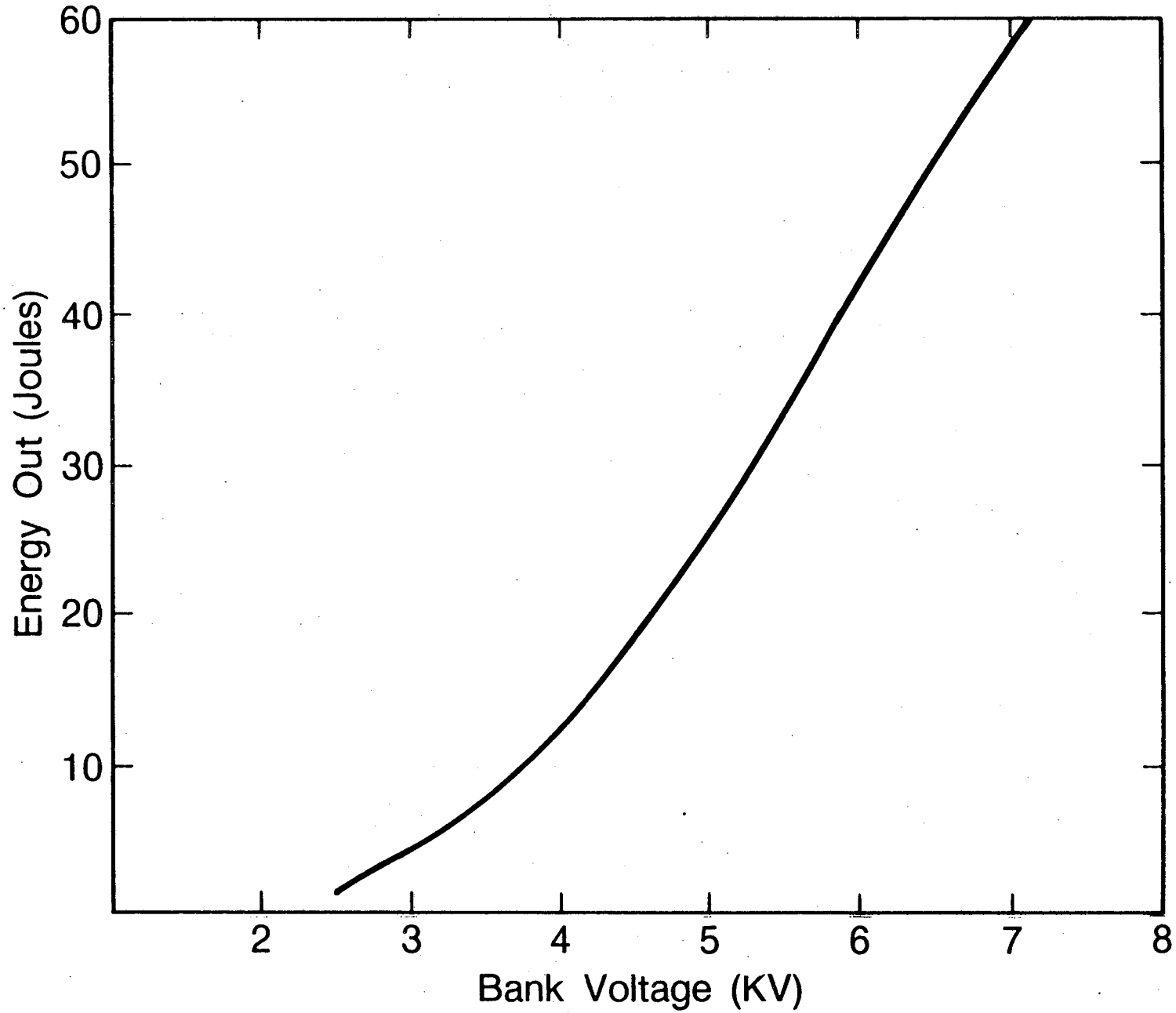

XBL 875-7743

Fig. 3.3

Tsai [1] and Tehranian [2] determined the intensity distribution by traversing an opaque knife-edge at 45° angle in the beam path and by measuring the energy of the chopped beam using a laser calorimeter. This method measures radial intensity distribution that is inherently averaged over the polar coordinate. The dimensional precision of this method is limited by that of the micrometer controlling the knife-edge motion.

In this work the intensity distribution was measured by a photographic technique. The method involved irradiating the laser beam on a glass plate coated with special Kodak emulsion (HSIR 2481). The maximum allowable exposure to this emulsion is 15 to 20 mJ/ cm^2. Therefore the intensity of the laser beam had to be cut down by a factor of 10^3. This was achieved by reflecting the laser beam from three separate low angle glass wedges before it was allowed to expose the emulsion plate. The emulsion plate was held in a special camera equipped with anti-reflection coatings that allowed only 1.06 μ m light to pass.

The exposed emulsion plates were analyzed by a special densitometer at Lawrence Livermore National Laboratory. The densitometer was capable of measuring and digitizing the exposure level on the emulsion plate as a function of position. A false-color image of the beam could also be generated by the densitometer where the light-colors show the regions of high exposure from the laser beam. Increasingly darker colors show lower degrees of exposure.

Several such exposures* of the laser beam were taken over a large range of high voltage applied to the capacitor banks of the laser power supply. From the false-color images, it was concluded that the laser beam is roughly circular with a diameter of ~ 1.7 cm. About 10% variation in the beam diameter was observed depending on the power supply

* See authors' paper "Surface Temperature Transients from Pulsed Laser Heating of UO_2", to be published in J. Nucl. Mater. for the false-color images of typical laser shots used in this work. This *color illustration* provides a normalized relative intensity map of the beam, time-integrated over the pulse duration.

setting. The beam intensity is nearly uniform for a given laser shot. The intensity distribution, although nearly uniform for a particular shot, varied spatially with the high voltage setting from one shot to other. These observations are consistent with the type of laser used in the present work.

Mathematically, the spatial intensity distribution is represented by the effective area, A_{eff} of a laser beam. It is the area of a hypothetical, spatially uniform laser beam with the same intensity as the peak intensity of the real beam and whose total energy is also equal to that of the real beam. From the digitized intensity as a function of position obtained from the densitometer, an integration can be performed to compute A_{eff} for a laser shot. An average value of 2.27 cm^2 was assigned to A_{eff} based on the estimates made on several shots.

1.3. Laser Irradiance

Laser irradiance, QP, is a useful quantity generally used to characterize laser beams. It is given by

$$QP = \frac{E}{A_{eff}\, t_{pul}} \tag{3.1}$$

and, by definition, represents the total energy contained in the pulse as well as the temporal and spatial characteristics of the pulse. QP governs the temperature rise of the target and the resulting number density of the vaporizing species in the ionizer. The output of the photodiode tube gives the temporal shape, which is normalized and integrated over the pulse width to compute quantity t_{pul} . The maximum value of the photodiode signal or the high voltage setting on the laser power supply can be used to obtain E (Figs 3.2 or 3.3). The laser irradiance, QP, is calculated by experimentally measured quantities appearing on the right hand side of Eq (3.1). Thus accuracy of QP calculated for a given laser shot depends on the experimental uncertainties associated with measuring these quantities.

2. DATA COLLECTION

Three transients are monitored simultaneously during laser pulsing of the target. These are the output signals from photodiode tube, pyrometer and mass spectrometer. All the three instruments are current sources; they deliver time-dependent current outputs that are proportional to the parameters they measure. If these outputs are fed directly into the waveform recorder with a 1 M Ω input resistance, the RC time constant considering a 10 foot long connecting cable of 25 pf/foot will be 250 μ s. Since the transient signals being measured occur over nearly 2 ms, the RC time delays are significant in the measurement of the transients.

The RC delays can usually be made negligibly small by using a appropriate terminating resistor. The terminating resistor, much smaller than the input resistance of the instrument, is applied in parallel. This lowers the effective input resistance of the instrument, making RC time constants acceptably small. This method has a disadvantage of simultaneously lowering the *magnitude* of the transient. Therefore it cannot be successfully used for RC correction of weak transients.

Only the photodiode tube signal could be properly RC-corrected by a 50 Ω terminating resistor. The transient signals from the pyrometer and the mass spectrometer became too small to be reliably measured with the use of the terminating resistors. Therefore, to avoid the need of analytical corrects, appropriate current-to-voltage converting preamplifiers were used for monitoring the latter two outputs.

The preamplifiers were located in the immediate vicinity of the output connectors of the mass spectrometer and the pyrometer. and were respectively rated at 1 μ amp/volt and 10 μ amp/volt. Fig 3.4 (a) and (b) show for the mass spectrometer and the pyrometer respectively a typical signal via preamplifier superimposed on the same signal without the use of the preamplifier. The RC delays are evident from Fig 3.4. The signals with and without the use of the preamplifier were found to be consistent with analytical RC corrections.

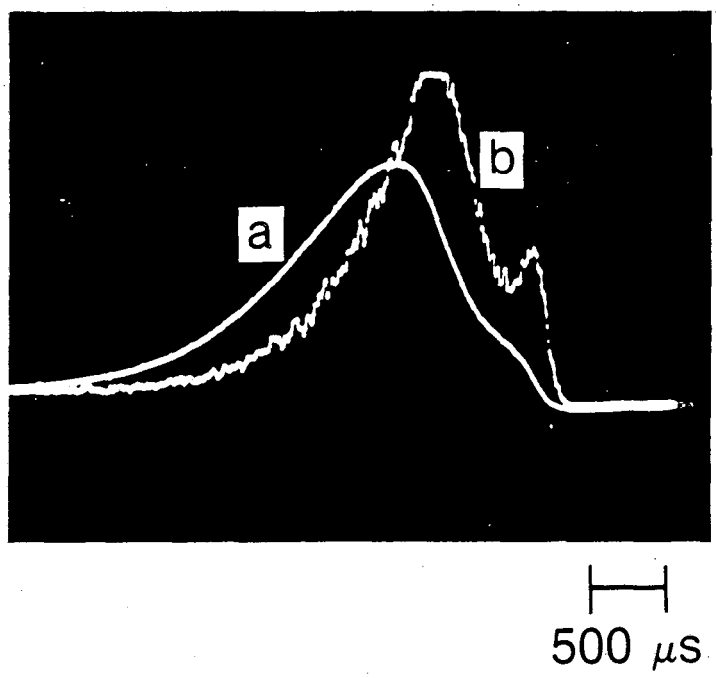

Mass Spectrometer

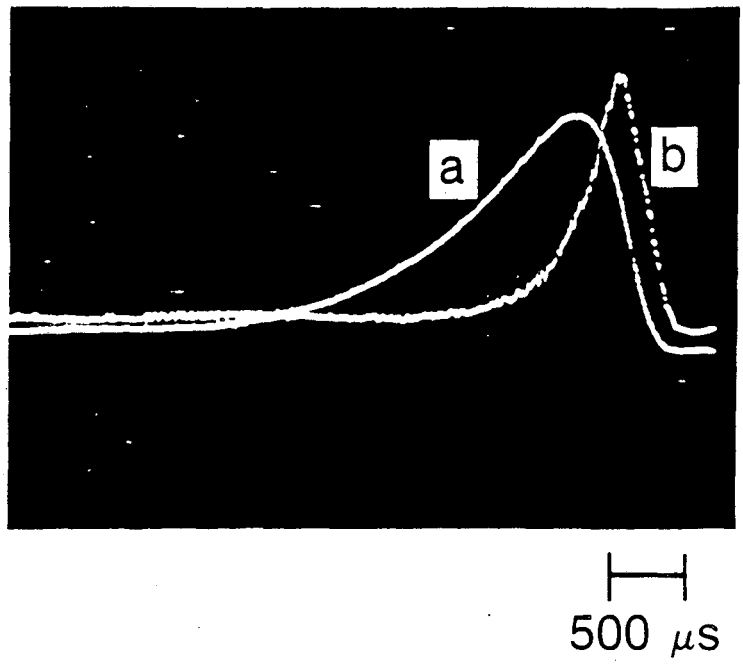

Pyrometer

Fig. 3.4

CHAPTER 4

TEMPERATURE MEASUREMENT

1. DESCRIPTION OF THE OPTICAL PYROMETER

The target surface temperatures were measured by a PYRO PHOTOMATIC Automatic Optical Pyrometer (Model A-164), manufactured by Pyrometer Instrument Company. The optical pyrometer was designed to respond to a narrow band of radiations at 0.65 μ m wavelength.

The instrument can be operated in several different modes [11]. In the "automatic" mode it can measure steady temperatures directly on a meter. The internal reference lamp in this mode is automatically adjusted to match the brightness of the target. Thus the function of a human eye in commonly used disappearing filament manual pyrometers is replaced by the internal circuitry in this "automatic" pyrometer.

In the "transient" mode the optical unit is coupled directly to a photomutiplier tube. In this mode the pyrometer delivers a current output that is a measure of the target temperature. The response time of the instrument, about a few nanoseconds, was negligibly small compared to expected temperature transients occurring over about two milliseconds. The electronic unit of the pyrometer was completely serviced since its use in the previous investigations [1,2] to ascertain proper functioning. Further, the photomultiplier tube of the pyrometer was modified so that its anode would accept even higher currents in shorter time durations. This insured that the photomultiplier tube would not "saturate" during rapid transients with high surface temperatures.

2. AVOIDANCE OF WINDOW COATING

The temperature was measured by the pyrometer by viewing the target through a window on the vacuum system. The window was equipped with an "on-off" flag to prevent it from being coated by the material vaporizing from the target. The flag served this purpose well

for intermittent low temperature measurements (e.g. mass spectrometer calibration). However, for laser pulsing experiments, where the window had to be left exposed and the temperature was higher, gradual coating of the window was observed. To circumvent this a carousel was designed to replace the "on-off" flag.

The carousel, shown in Fig 4.1, consists of two copper cones attached to a flange on the vacuum system. The inner cone has a circular hole cut on its conical surface, whereas the outer cone has several such holes with sacrificial transparent glass plates attached to each. The hole on the inner cone is aligned with the pyrometer line of sight of the target. By rotating the outer cone, fresh glass plates are exposed one at a time, preventing coating of the vacuum system window. The addition of the carousel assured correct temperature measurements; free of any error caused by the window coating problem.

3. PYROMETER CALIBRATION

A THERMOGAGE dual pyrolytic graphite blackbody cavity at NASA-Ames Research Center was used as a high temperature source for calibrating the pyrometer. The source temperature was measured by a disappearing filament manual pyrometer, used as a "standard". The "standard" pyrometer's calibration was traceable to the National Bureau of Standards [12]. The pyrometer to be calibrated is focused on the same spot in the cavity as the "standard" pyrometer.

Since the fast automatic pyrometer can be operated in "automatic" and "transient" modes, it was calibrated in both these modes. For the "automatic" mode the maximum *internal* high voltage setting was used and the blackbody source temperature was calibrated against the meter reading of the pyrometer (Fig 4.2).

In the "transient" mode, two different calibrating procedures were used. First, the calibration procedure given in pyrometer's manual [11] was employed. This involved measuring d.c. output from the pyrometer as a function of blackbody temperature for different values of *external* adjustable high voltage settings. The second method of "transient" mode calibration involved simulation of temperature transients by a

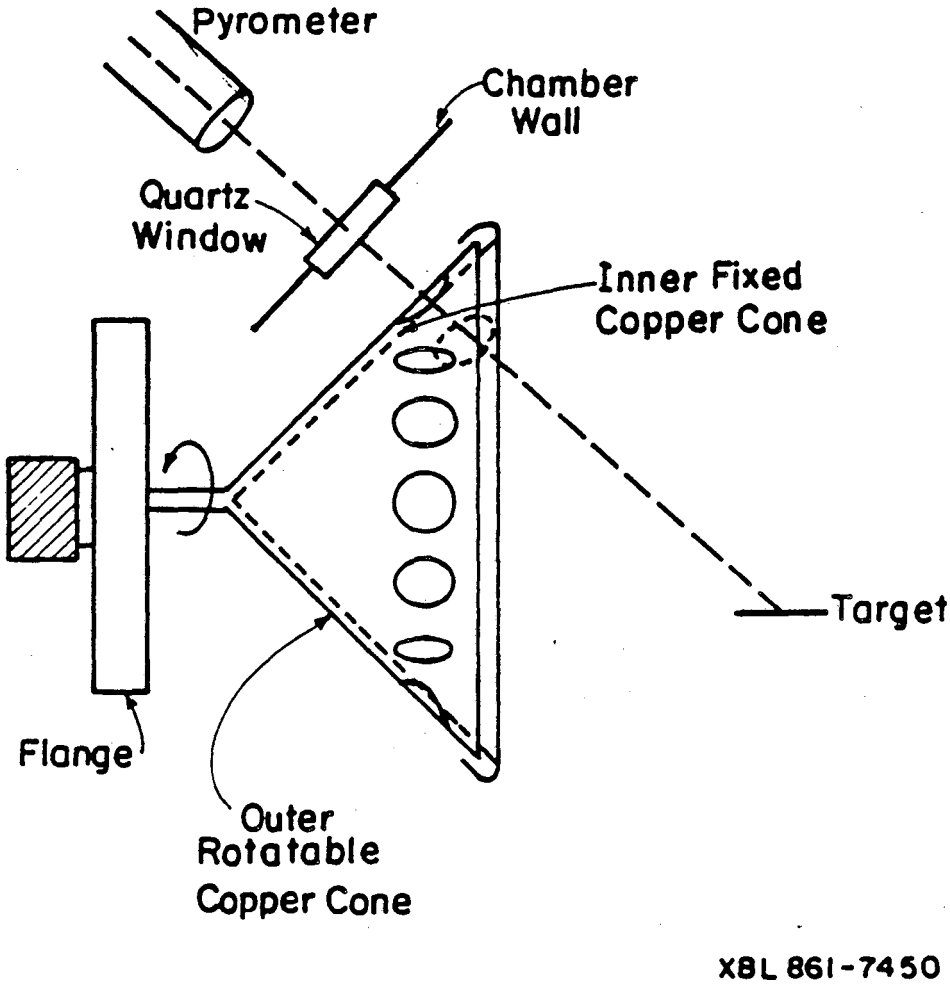
Pyrometer
Chamber Wall
Quartz Window
Inner Fixed Copper Cone
Target
Flange
Outer Rotatable Copper Cone
XBL 861-7450

Fig. 4.1

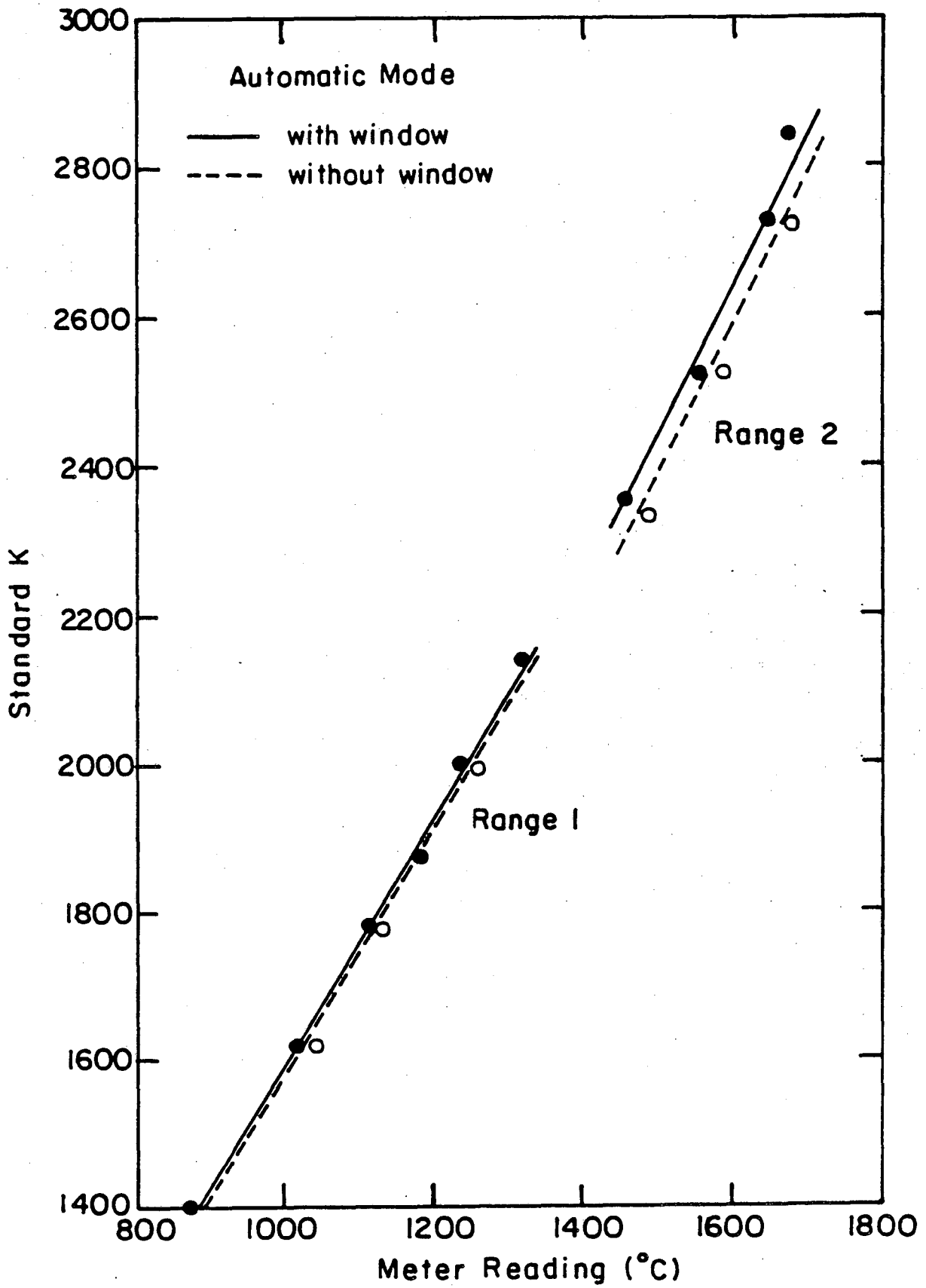

XBL 861-7451

Fig. 4.2

chopper wheel placed between the blackbody source and the pyrometer. Under this simulated temperature transient condition, the pyrometer output via a preamplifier was monitored on a waveform recorder. In the latter method, calibration conditions were identical to those encountered in the experiment with laser pulsing except for the means of generating the temperature transient.

The calibration results from these two methods were found to be consistent with one another when the rated amplification of the preamplifier and the input resistance of the oscilloscope that was used in the conventional method were accounted for. This assured that the pyrometer functions properly during transients and that the first method of calibration is sufficiently accurate.

Figs 4.3 - 4.5 show the calibration lines of the pyrometer in the "transient" mode for three different ranges of the pyrometer. The *external* bias voltage is also shown for each calibration line. The attenuation in the pyrometer output because of the vacuum system window and the carousel glass plate is built into Figs 4.3 - 4.5. There is some scatter in the calibration points between repeated calibration attempts, especially in range 3. If the output voltage is measured accurately, an error of ± 50 at 2500 K in measured temperatures can be inferred from the calibration data. Considering other uncertainties, such as lack of emissivity data, this error limit in the measured temperature is acceptable.

4. VALIDATION OF MEASURED TEMPERATURES

4.1. Comparison of Measured and Computed Temperatures

Surface temperature history of a laser heated target can be computed by solving appropriate energy balance equation. This requires the knowledge of the physical, thermodynamic and transport properties of the target material and the characteristics of the laser pulse. Muzaffar [13] performed such numerical solutions. The model for his calculation was that of a semi-infinite solid undergoing surface heating. Melting and Hertz-Langmuir ablation was included but one-dimensional heat conduction was assumed.

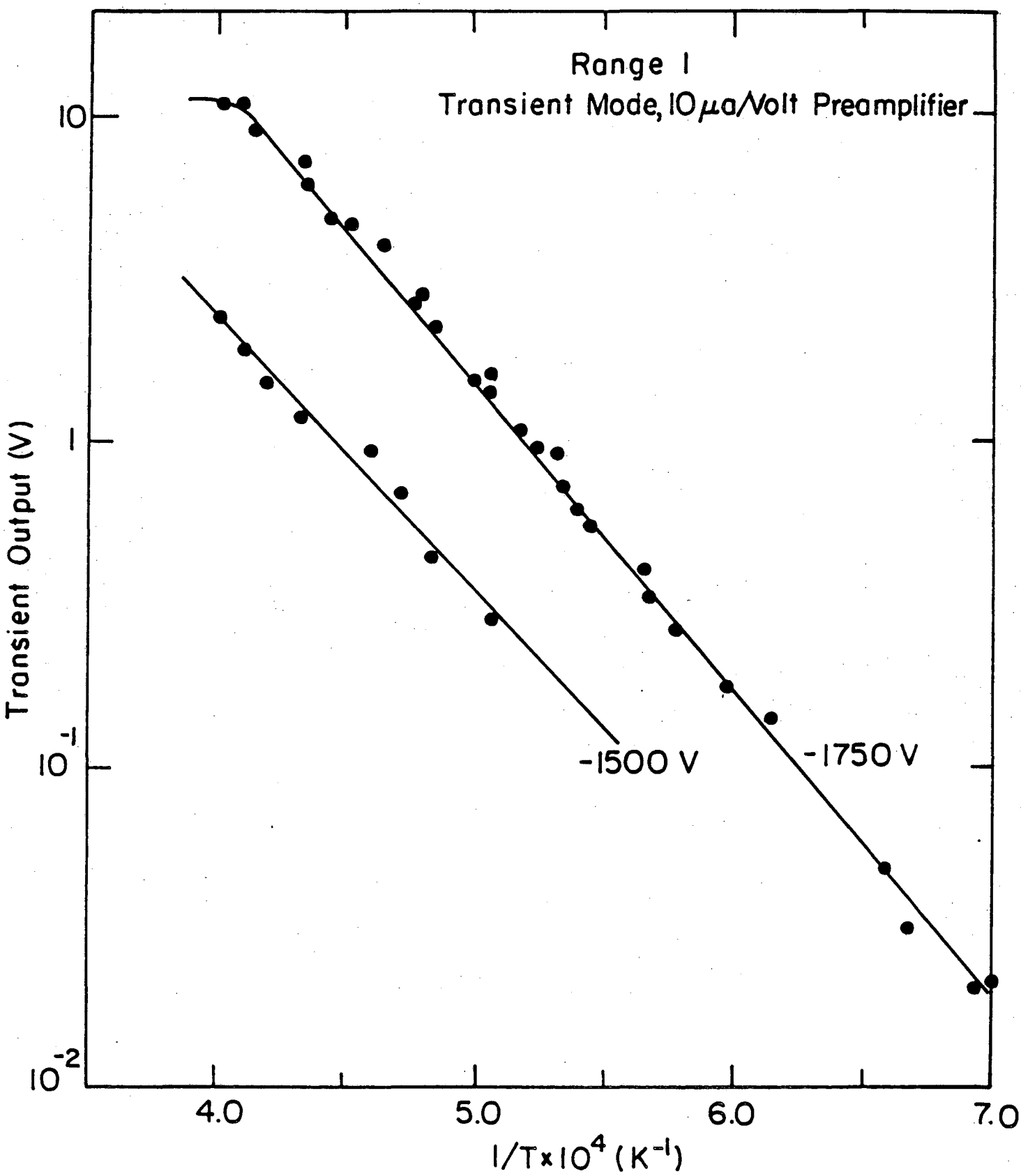

Fig. 4.3

XBL861-7452

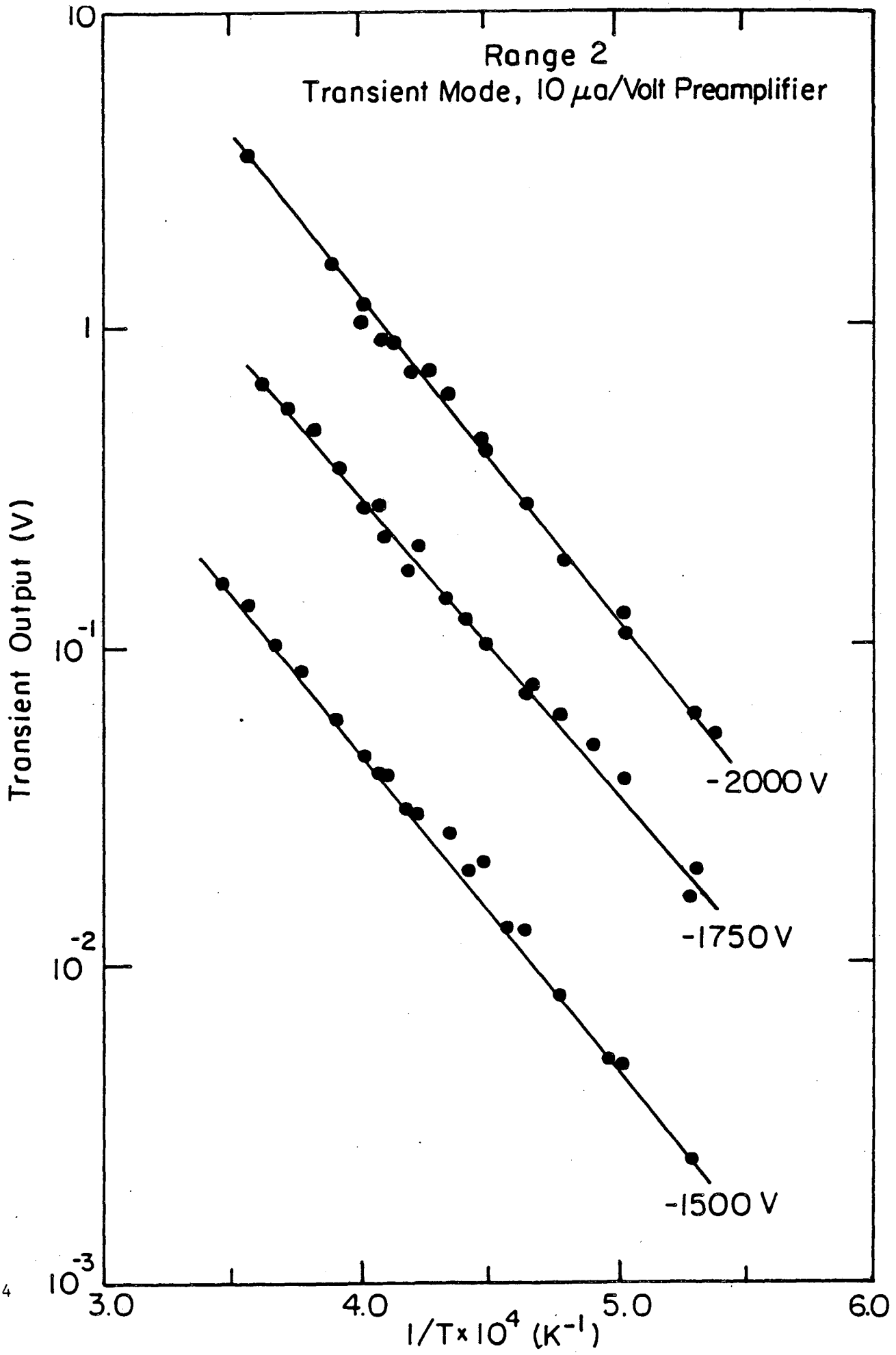
Range 2
Transient Mode, 10 μa/Volt Preamplifier
Transient Output (V)
10
1
10^-1
10^-2
10^-3
3.0
4.0
5.0
6.0
1/T x 10^4 (K^-1)
-2000 V
-1750 V
-1500 V

Fig. 4.4

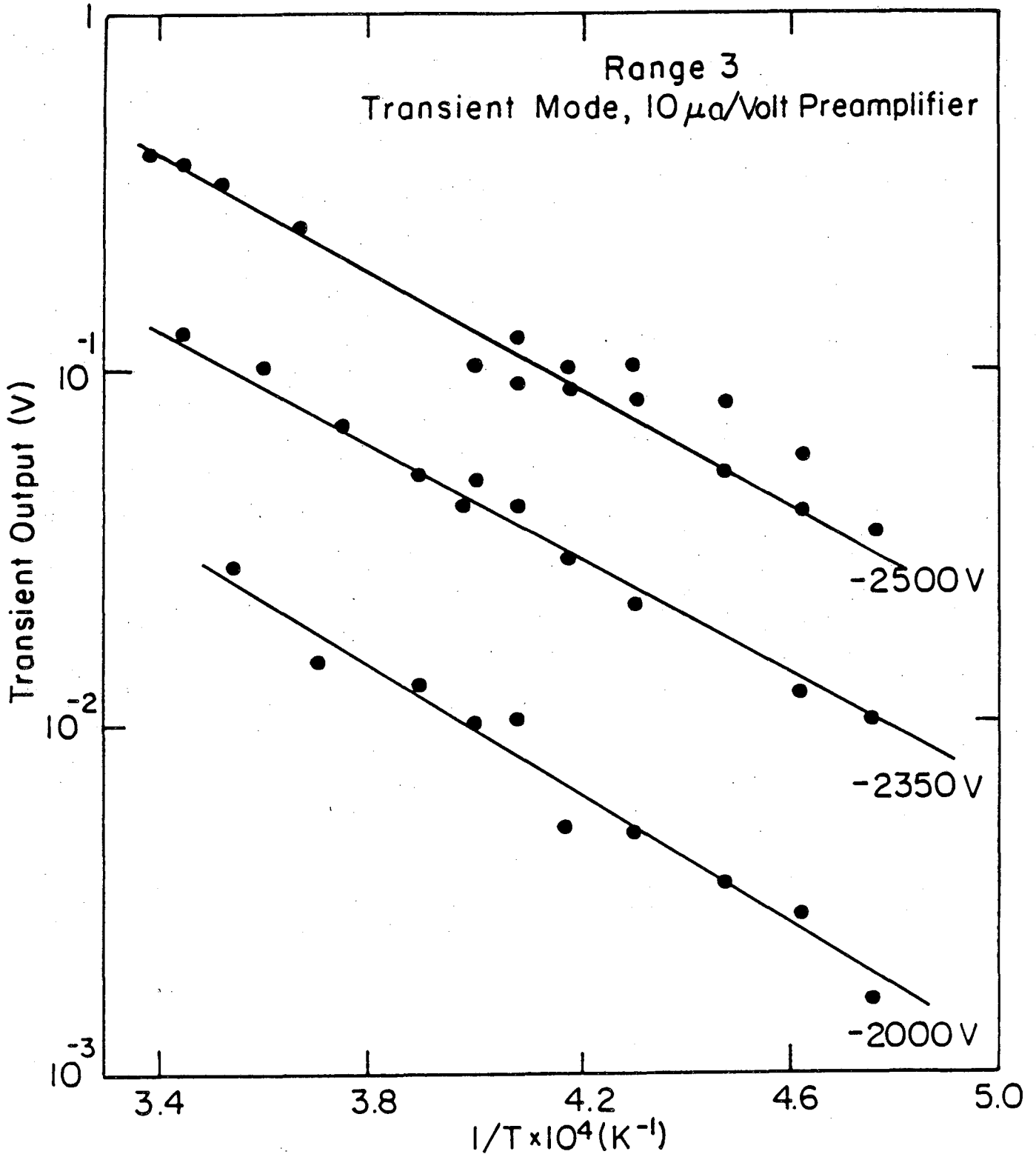

XBL 861-7454

Fig. 4.5

The key input parameter of Muzaffar's computer code is the laser irradiance, QP. QP was calculated from Eq (3.1) with the energy E inferred* from Fig 3.3. The variations in the laser pulse width with the applied input power (section 1.1, Chapter 3) was ignored in Ref [13]. The code has since been modified to accept this variation.

The laser irradiation intensity, QP, was varied between 10^3 to 10^5 W/cm^2 by varying the electric charge applied to its power supply. In this way UO_2 target temperatures of nearly 3700 K were obtained with the unfocused laser beam as measured by the optical pyrometer [11].

An acceptable agreement existed between the measured and the computed maximum surface temperatures (Table 4.1) In addition, the temperature histories of the measured and the computed temperatures matched well, particularly the time of maximum surface temperature [13]. This is shown in Fig 4.6 where the measured and computed normalized temperatures, i.e., $(T_s(t) - T_0) / (T_{smax} - T_0)$ is plotted as a function of time.

Some scatter in the measured maximum surface temperature, T_{smax}, was observed for the same nominal QP. This can be attributed partly to the fact that the intensity distribution of a multi-mode laser beam is known to vary spatially from one shot to another [9]. It should be noted that the pyrometer measures an averaged target surface temperature over its view-spot on the target (~ 2 mm in diameter) while the laser beam (diameter 1.7 cm) heats the entire target surface. Therefore the spatial intensity variations (occurring randomly from one laser shot to another) could cause the scatter in the measured temperature for the same nominal QP. Secondly, since the laser pulse width and its temporal shape varies from one pulse to another, variations in measured maximum temperature for a given nominal value of QP are expected to

*If E was inferred from Fig 3.2 instead, the corresponding values of QP would have been nearly half of those based on Fig 3.3. However, as further discussed in this section, the former method of computing QP would result in a poor agreement between the measured and the computed temperatures. This was among several reasons to suspect the photodiode tube calibration of Fig 3.2.

TABLE 4.1

Comparison of Measured and Calculated Surface Temperature

Laser Power Supply Setting, kV	QP, 10^4 W/cm^2*	Maximum Surface Temperature, K		Difference
		Measured	Computed**	
8.0	6.374	3648	3676	- 28
7.5	5.539	3666	3572	+ 84
7.0	4.103	3513	3326	+188
6.5	3.767	3213	3194	+ 19
6.0	3.371	3130	3059	+ 71
5.5	2.453	2906	2795	+111
5.0	1.910	2666	2571	+ 95
4.5	1.358	2379	2294	+ 85

* Fig. 3.3 was used to determine E; QP calculated from Eq(3.1) using t_{pul} determined from individual temporal shape of the pulse and $A_{eff} = 2.27$ cm^2.

** SURFT3, modified version of SURFT2 [13].

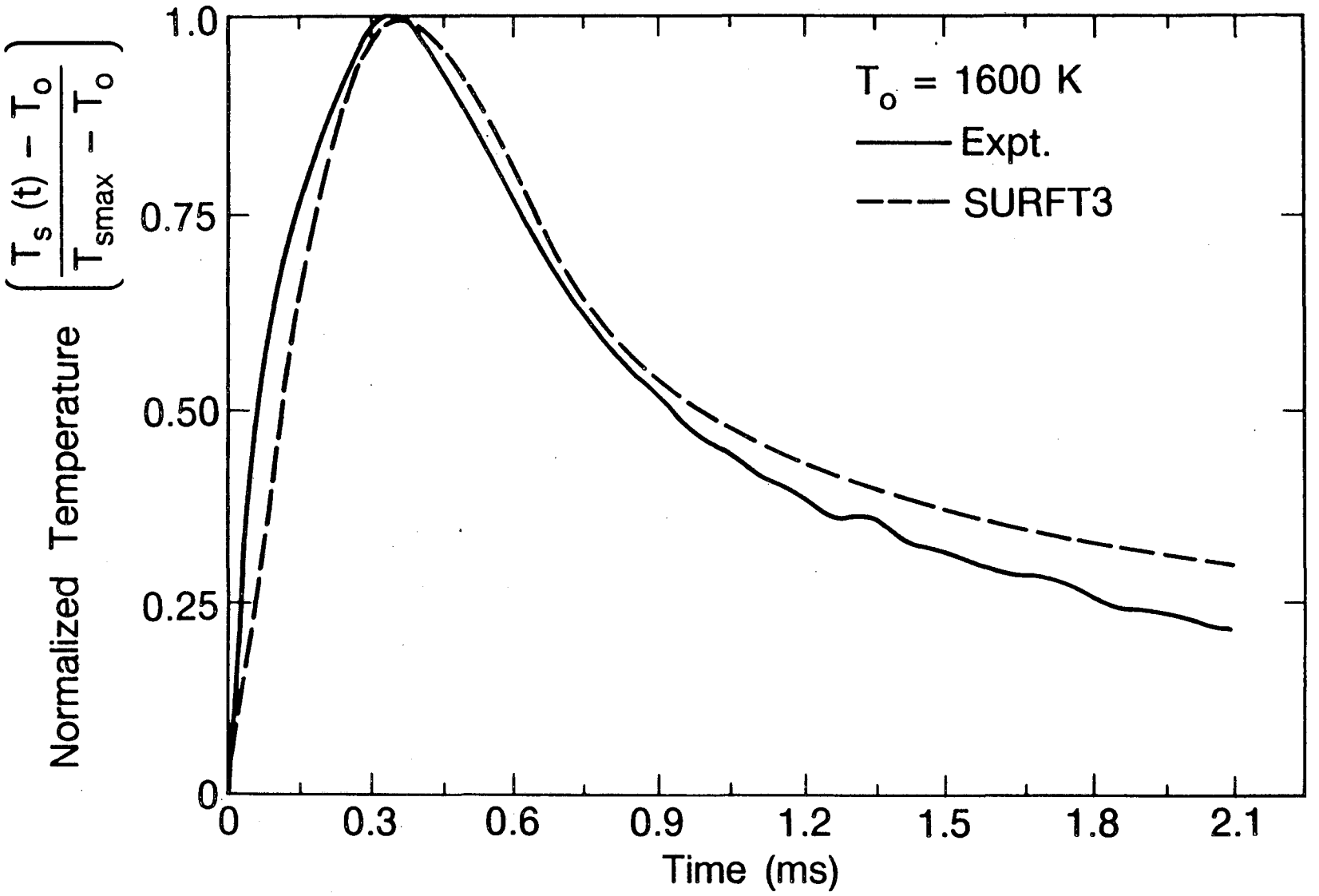

Fig. 4.6

XBL 875-7742A

occur.

Tests were done to check whether the measured temperatures were indeed reasonably accurate. Several polished UO_2 targets were each fired with a single laser shot at preselected values of QP. The target surface were examined under scanning electron and optical microscopes. Based on the evidence of melting on the surface the measured temperatures were accepted. For example, Fig 4.7 shows a photomicrograph of the surface irradiated with a single laser shot of $QP = 6.4\times10^4$ W/ cm^2 where the measured T_{smax} was 3676 K as compared to the computed value of 3648 K. The slight disagreement between the measured and the calculated temperatures was ignored.

4.2. Luminosity of Vapor Plume

In another set of tests, the pyrometer response was monitored when sighted on regions in front of the target surface because of concern over luminous vapor plume that *might* exist ahead of the vaporizing surface. Luminous vapor-plumes have been observed when the laser-heated solid is in an ambient gas (see for example Refs [9,14]). Radiations from such luminous vapor-plume could result in possible inaccuracies in the temperature measured by the pyrometer. The two-color pyrometer used in a recent work reported by Bober and Singer [15] had better than ±15 K accuracy at 3000 K. However, the authors suspected a much greater uncertainty in real measured temperature of the target surface. This was stated to be due to two reasons. The first reason was the uncertainty in the spectral emissivity of the target surface and the second one was the presence of luminous vapor plume arising from the target surface. The pyrometer measurements were suspected to be disturbed by the radiations emitted from the vapor plume. In the present work, however, the latter reason can be ruled out. Since no inert gas back-pressure was used in the target chamber, the luminous plume does not exist. Secondly, the the measured temperatures were found to be reasonably accurate based on the target-surface melting tests described earlier in this chapter.

Although for a solid vaporizing in high vacuum, such as in this work, a luminous vapor-plume is generally not anticipated, an attempt,

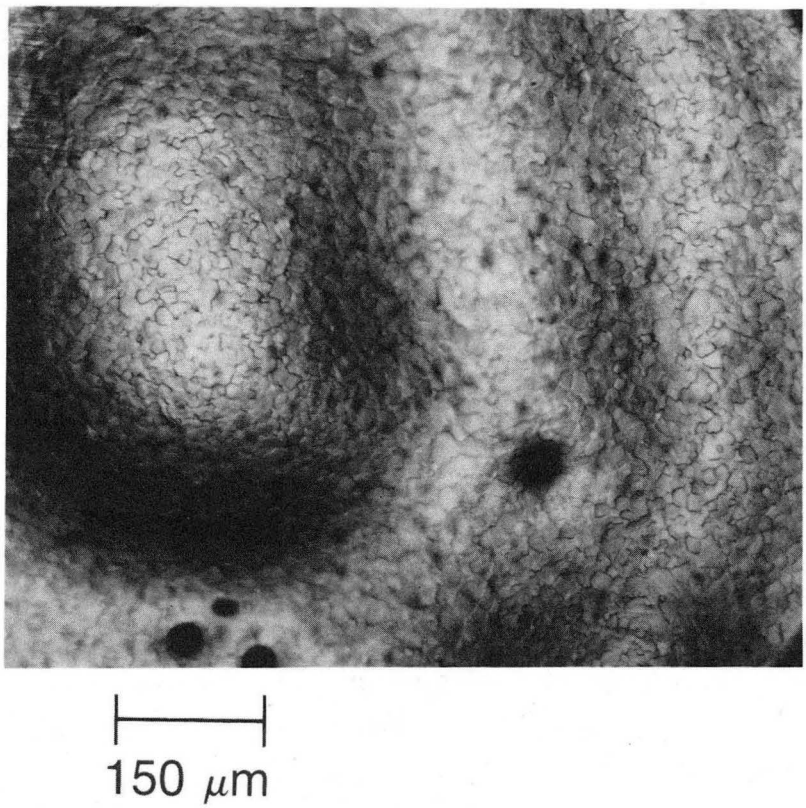

XBB 870-8535

Fig. 4.7

however, was made to measure the response of the pyrometer when sighted on the region where vapor-plume exists during laser pulsing. The results of these measurements for UO_2 and graphite targets are discussed below.

Two locations (marked A & B in Fig 4.8) which were about 2 to 3 cm apart, in roughly perpendicular direction to the target surface were chosen for these measurements. A third location(C), clearly away from vapor flow path, was also selected for graphite target. The location nearest to the target surface was chosen to just avoid the target holder from field of view of the pyrometer. Any signal registered by the pyrometer at these locations during laser pulsing of the target is a measure of the interference that the instrument receives due to the luminosity of the vapor-plume or some spurious reflections of the laser light.

In Fig 4.8, the maximum of the transients (in volts) "measured" at these locations are compared to the the maximum signals obtained when sighting the target surface directly during a laser pulse. The maximum target surface temperature, T_{smax} , was increased by increasing the laser irradiance. The computed values of T_{smax} assume constant emissivities for the two target materials.

The data in Fig 4.8 suggest that at low T_{smax}, where the vapor number densities are low, the pyrometer response is unaffected by the location of sighting. It is also nearly three to four times lower than the signal strength measured by sighting the target surface in normal fashion. However, for strong laser pulses giving T_{smax} beyond the melting point of UO_2, the signal increases with the proximity of the sighting location, i.e., a location closer to the target surface, where the vapor density is higher, does tend to register a larger signal compared to a location far removed from the surface. A similar response was observed for graphite target as well. Nevertheless, this interference signal is more than an order of magnitude lower compared to the signal measured by sighting the target surface directly. Therefore it was concluded that errors introduced in the measured temperatures due to luminosity of the vapor plume are negligible.

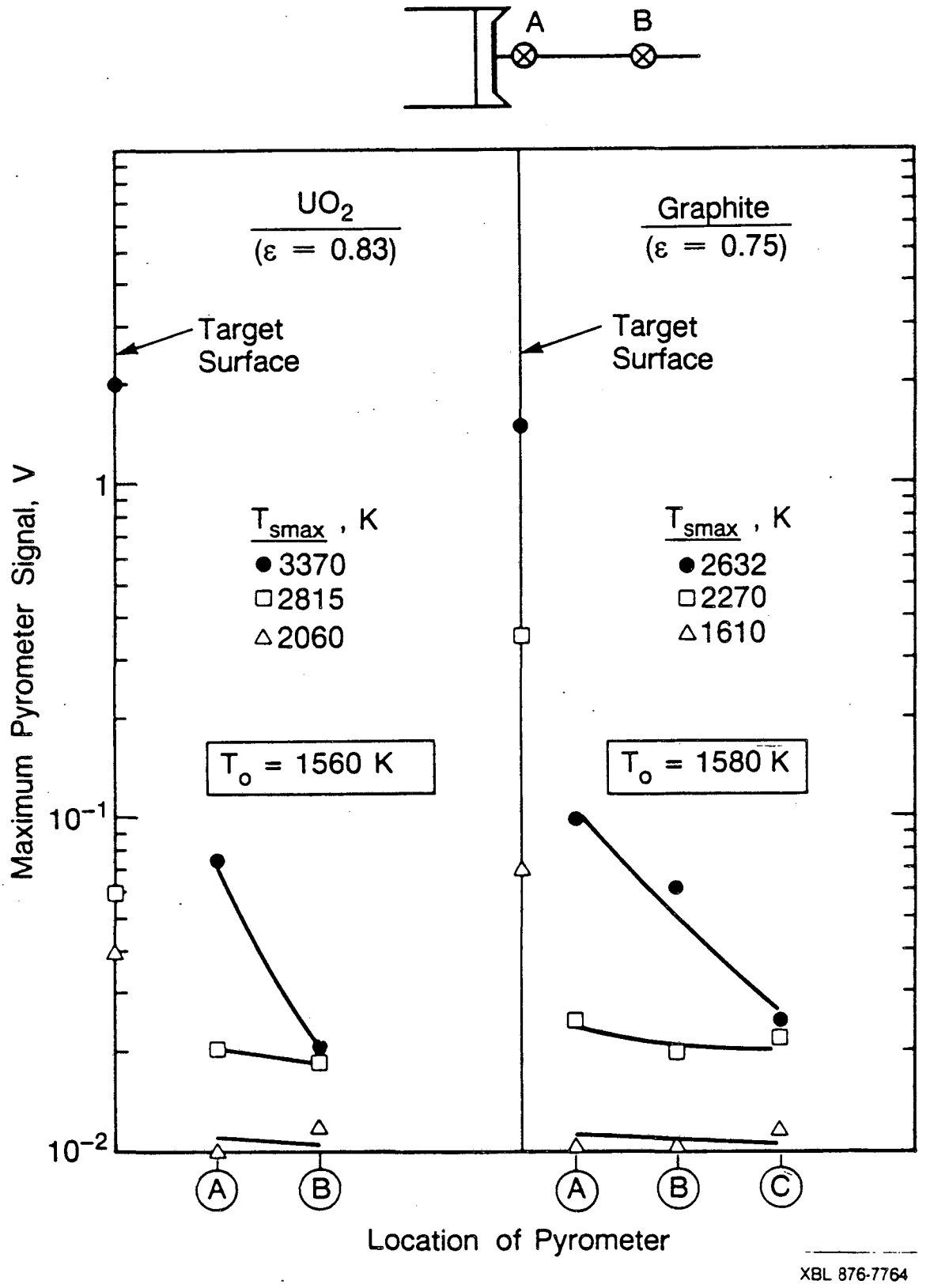
A
B
UO2
(ε = 0.83)
Graphite
(ε = 0.75)
Target Surface
Target Surface
Tsmax , K
3370
2815
2060
Tsmax , K
2632
2270
1610
To = 1560 K
To = 1580 K
Maximum Pyrometer Signal, V
1
10−1
10−2
A
B
A
B
C
Location of Pyrometer
XBL 876-7764

Fig. 4.8

CHAPTER 5

THE MASS SPECTROMETER RESPONSE

For accurate, reproducible measurements with the mass spectrometer, it is important to correctly tune the instrument to species being detected. For this purpose, the mass spectrometer control unit has rotatable-dial type potentiometer-pots controlling the mass-to-charge ratio. Thus the potentiometer dial setting needs to be calibrated with species of known mass numbers over a wide range. This calibration is then used to "detect" the species of interest. The organic liquid perfluorotributylamine, manufactured specially for mass spectrometric applications by PCR, Incorporated [16] was used to do this calibration.

Vapors from this liquid were introduced into the mass spectrometer chamber via a one quarter inch stainless steel tubing. Several peaks corresponding to different fragmentation species of perfluorotributylamine were observed on the mass spectrometer. The potentiometer dial setting corresponding to each of these species was noted as shown in Fig 5.1. The interpolated locations of the uranium bearing species are shown in Fig 5.1. The specified [16] relative intensities of different mass number peaks were found to be in good agreement with those measured. However, no peak corresponding to mass number higher than 502 was observed because of the limitations of the mass spectrometer.

There were two additional major concerns regarding the performance of the mass spectrometer during laser pulsing of the target. These were referred to in sections 4.3 and 4.4 of Chapter 2. In this Chapter measurements, which were done especially to determine the response of the mass spectrometer will be described. The information gathered by these measurements helped evaluate the mass spectrometer output signal from the laser pulsing experiments.

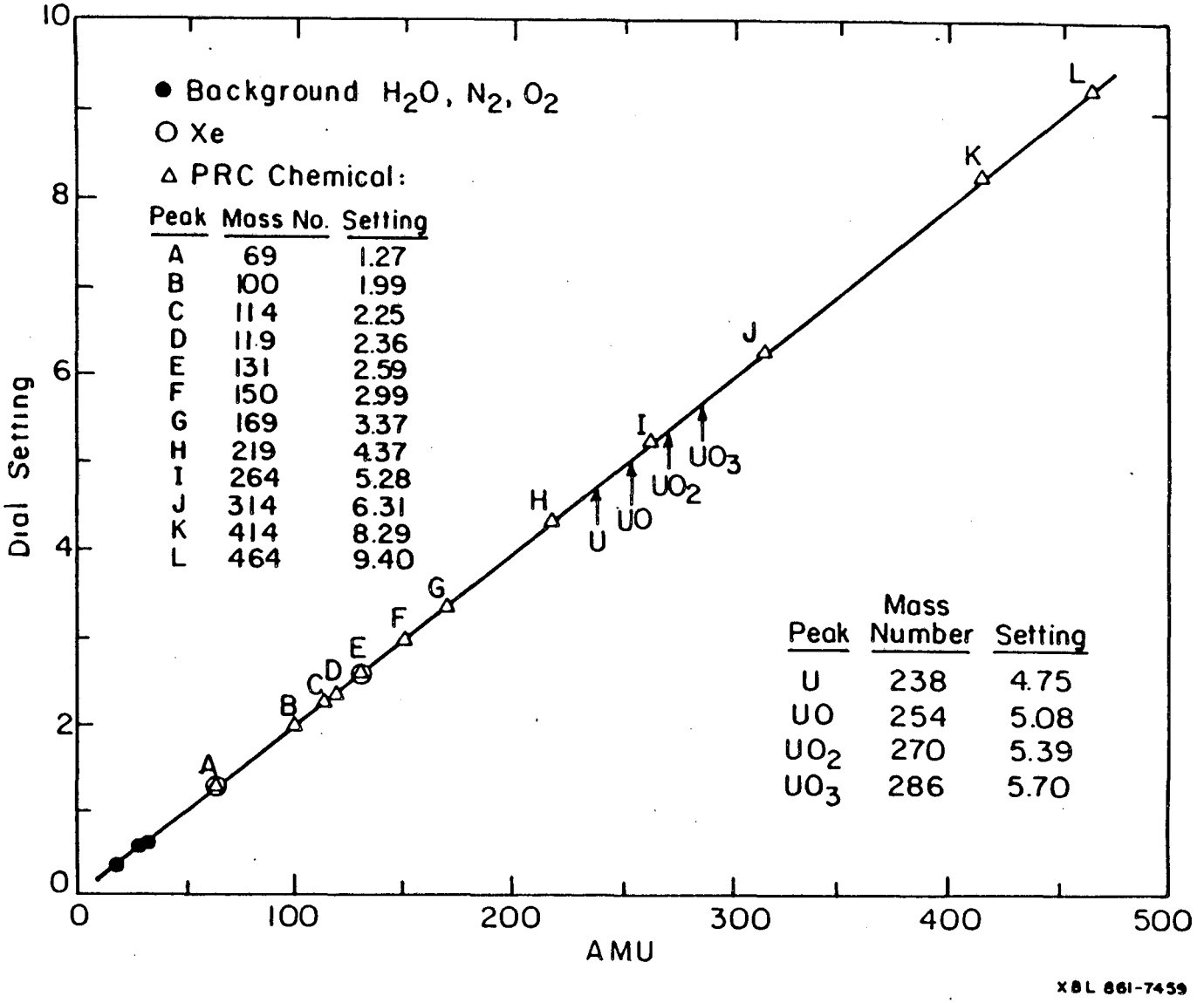
● Background H_2O, N_2, O_2
O Xe
△ PRC Chemical:
Peak Mass No. Setting
A 69 1.27
B 100 1.99
C 114 2.25
D 119 2.36
E 131 2.59
F 150 2.99
G 169 3.37
H 219 4.37
I 264 5.28
J 314 6.31
K 414 8.29
L 464 9.40
Peak Mass Number Setting
U 238 4.75
UO 254 5.08
UO_2 270 5.39
UO_3 286 5.70
Dial Setting
AMU
0
2
4
6
8
10
100
200
300
400
500
A
B
C
D
E
F
G
H
I
J
K
L
U
UO
UO_2
UO_3
XBL 861-7459

Fig. 5.1

1. MASS SPECTROMETER MALFUNCTION

The possibility of mass spectrometer malfunction was investigated on two fronts. First, the linearity of the mass spectrometer with respect to the equivalent pressure or number density of a given species in its ionizer was checked. Second, the stability of various current and voltage settings of the instrument's controller during laser pulsing was tested. Both these tests will be described below.

1.1. Nitrogen Doser Tests

These tests were intended to check the linearity of the response of the mass spectrometer as a function of number density in its ionizer. Pure dry nitrogen was introduced in the mass spectrometer chamber through a one quarter inch stainless steel tubing. The nitrogen beam was aimed at a metal strip inside the chamber to scatter the gas molecules randomly in all directions. The chamber pressure, measured by an ion-gauge tube, was thus assumed to represent the nitrogen pressure P_{eq} in the ionizer which is equivalent to that from a directed molecular beam.

The experimental set-up is schematically shown in Fig 5.2. P_{eq} was varied between 10^{-7} torr to nearly 10^{-3} torr. The resulting nitrogen signals from the mass spectrometer were measured on a waveform recorder. Controller settings of the mass spectrometer such as emission current in the ionizer and the high voltage applied to the electron multiplier were also varied in these tests.

Fig 5.3 shows the magnitude of the mass spectrometer signal as a function of P_{eq} for a fixed value of the emission current and three different high voltages applied to the electron multiplier. In Fig 5.4 the same quantities are plotted for a fixed high voltage and three different values of emission current. In the low pressure region of Figs 5.3 and 5.4, the data points fall nearly along lines of slope 1. Changing emission (or high voltage) simply changes the magnitude of the output signal in the region where the slope of unity corresponds to linear behavior of the instrument. As P_{eq} is increased, the output tends to level and really

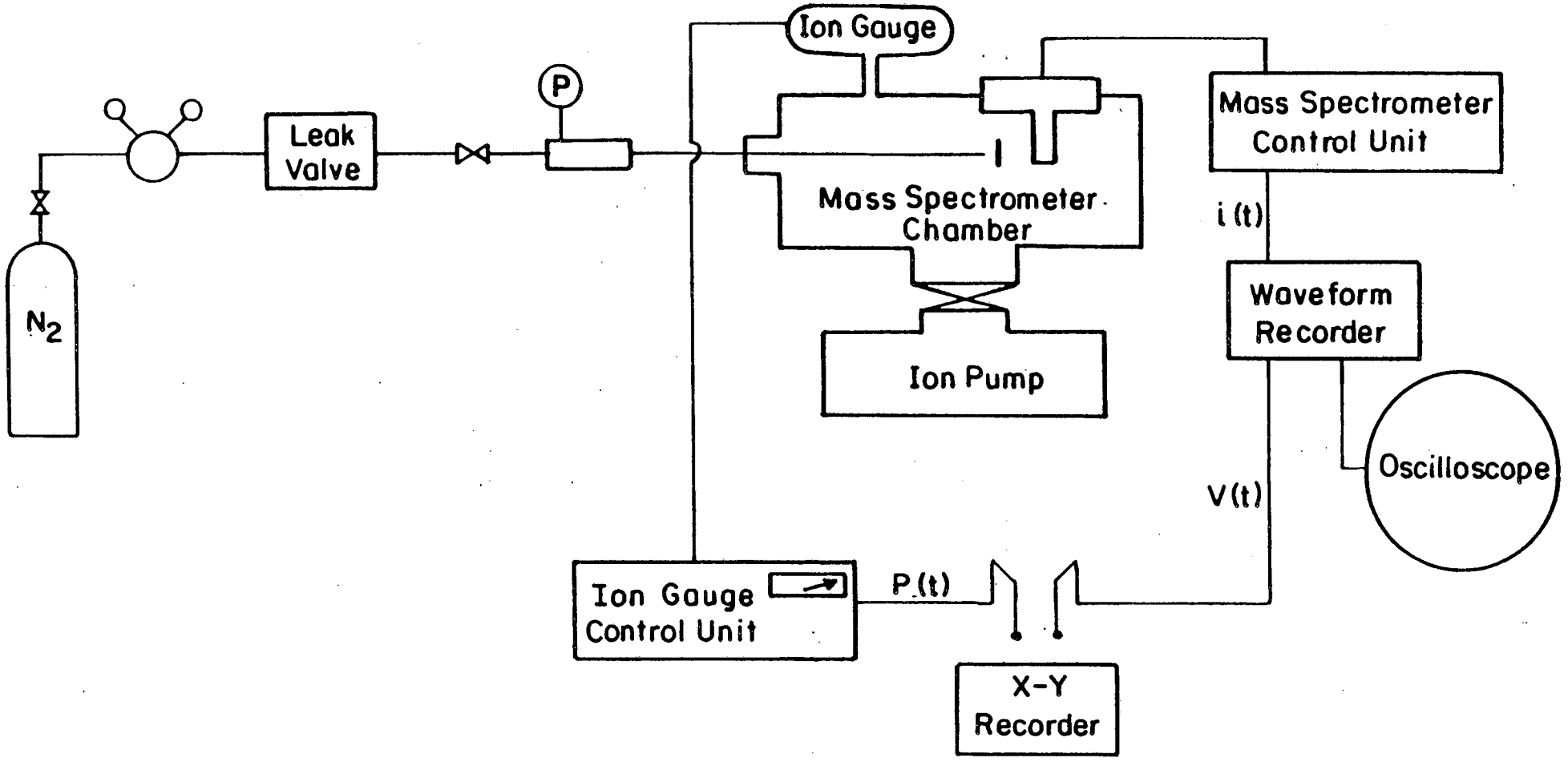

XBL 861-7456

Fig. 5.2

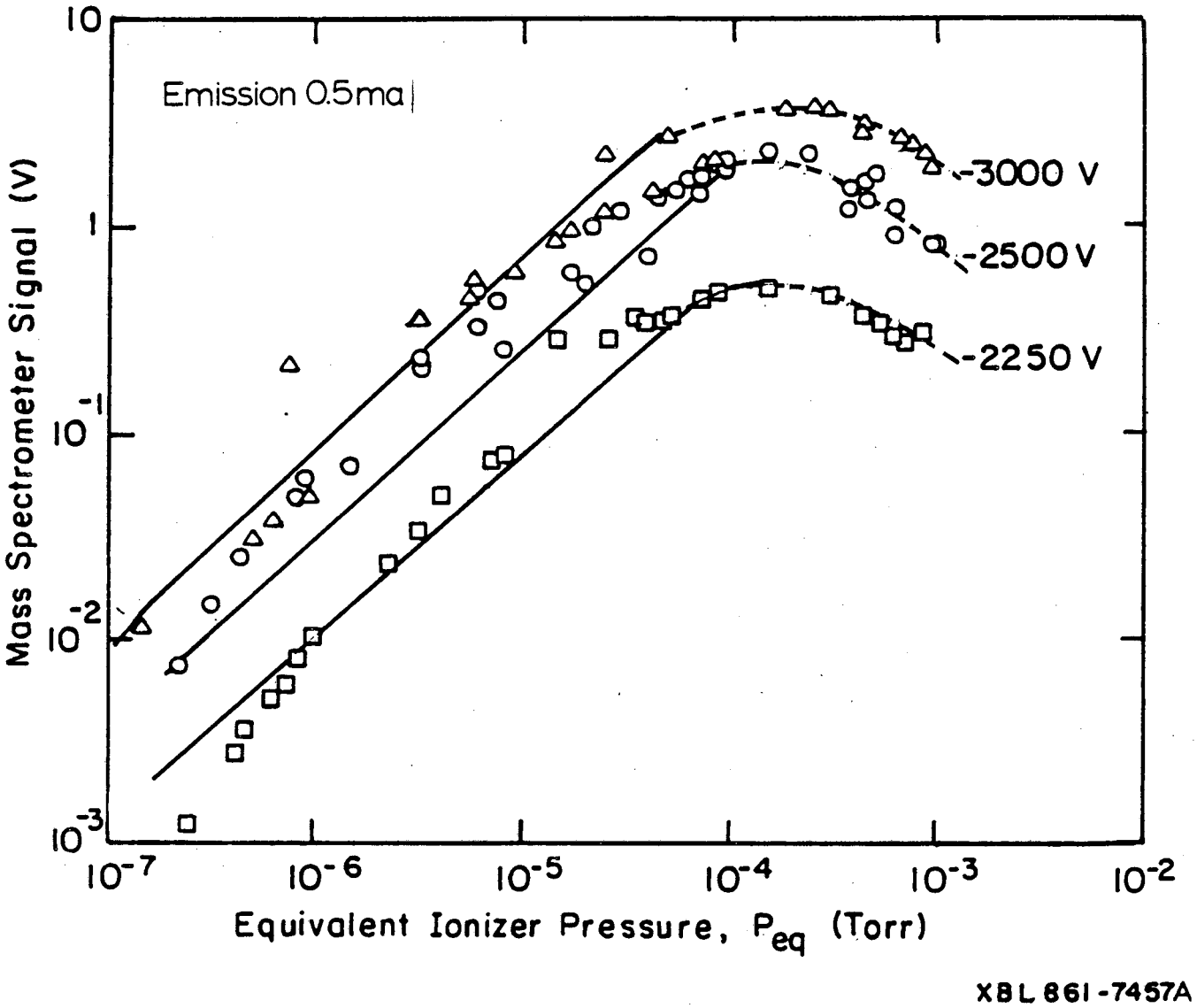

XBL 861-7457A

Fig. 5.3

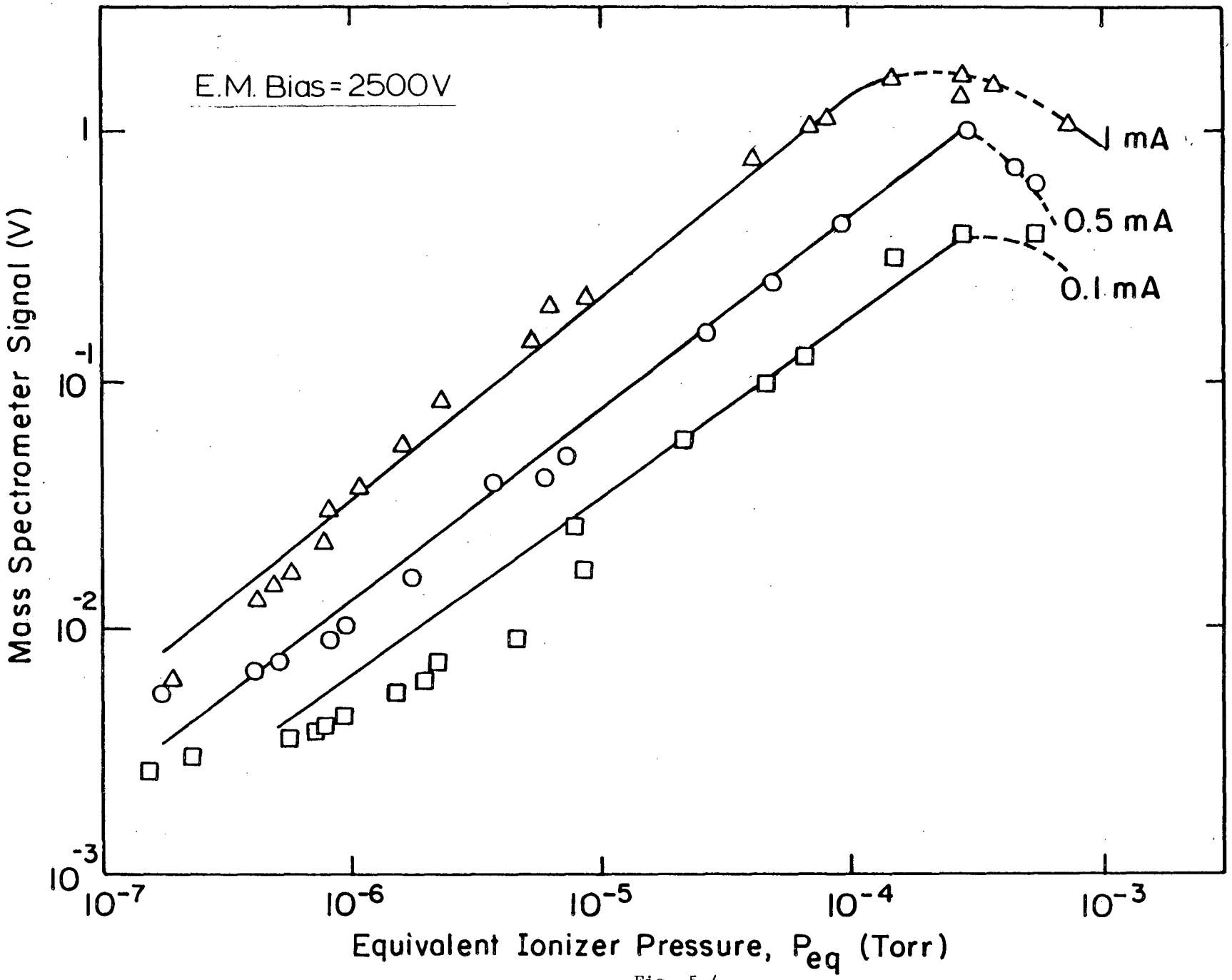

Fig. 5.4

XBL 861-7458A

decreases at ~ 10^{-3} torr pressure. The signal no longer remains linear beyond 10^{-4} . Such a break-down in linearity was expected since the mass spectrometer is designed for low-pressure applications only.

A P_{eq} of 10^{-4} is equal to a number density of about 10^{13} molecule/ cm^3. This limiting number density depends on the vapor species, and is probably lower for molecules such as UO_2 and UC than it is for N_2 . For UO_2 , it would require a target heated to about 3700 K to produce a number density of 10^{13} in the ionizer. The maximum number densities in the experiments of Tsai [1] and Tehranian [2] probably exceeded the linear range of the mass spectrometer. However, the deviations from the expected mass spectrometer response occur at surface temperatures ~ 2500 K.

1.1.1. Entrance Screens for the Ionizer

In another test for linear instrument response, the number density in the ionizer was artificially decreased by nearly an order of magnitude by interposing a screen between the collimator and the ionizer. The screen, fabricated of a metal strip with spark-cut parallel slits, can be positioned such that the ionizer "sees" only partial molecular beam coming from the collimator. During laser-pulsing tests on UO_2 , it was found that the mass spectrometer's output signal was reduced by exactly the factor corresponding to the percent open area of the screen. This indicates that the instrument is not saturating.

1.2. Stability of Controller Settings

Several important voltage and current settings are adjusted to optimize mass spectrometer output. These include ionizer filament current and emission, electron collector and focusing plate voltages. It appeared possible that either the RF field generated during laser shots or high-energy ions generated by laser irradiation on the UO_2 target might have perturbed these settings falsifying the output at the mass spectrometer. To check the stability of these settings, appropriate points in the instrument's controller circuitry were probed and the output from these probe points were recorded on a transient wave-form recorder

during routine operation of the mass spectrometer for the experiments. All these key currents and voltages were found to remain unperturbed.

As an additional check, the number density of some background gas species in the vacuum chamber were also monitored by the mass spectrometer *during* laser pulsing of the target. The output from the spectrometer for these background gas species remained at a constant level. Had the controller settings been perturbed because of the above mentioned or other plausible reasons, a corresponding perturbation in the output for the background gas species would have been observed.

2. COLLIMATOR EFFICIENCY

The mass spectrometer responds to molecules emitted from all positions on the 1-cm diameter heated target surface. However, because of the target- collimator- detector geometry, the response is not the same for all radial positions on the surface. That is, a molecule emitted from the center of the target has a greater chance of detection in the mass spectrometer than the one emitted from an off-center location. This effect is quantitatively accounted for by a function termed the collimator efficiency.

The definition of collimator efficiency is as follows:

$w(r)=$

relative probability that a molecule emitted from radial position r on the target surface becomes an ion and enters the quadrupole analyzer. By definition $w(0) = 1$.

The assumption used by Tsai [1] and Tehranian [2] was $w(r) = 1$ for $0 \le r \le R_c$, where R_c is the collimator diameter* , and $w(r) = 0$ for larger values of r. This assumption corresponds to a geometry where the *collimator* is placed directly over the vaporizing surface.

---

* For $R_c = 0.5$ mm , the correct value of the geometric factor K_g in Eq. (2.1) with this assumption should be 3.90×10^{-7} , *not* $K_g = 3.90 \times 10^{-5}$ reported on page 53 of Ref [1]. This error caused a factor of 100 discrepancy in Tsai's final results for UO_2 vapor pressure.

Tests involving partial masking of the vaporizing surface are needed to determine this function. Ohashi and coworkers [17] experimentally determined the collimator efficiency in the target- collimator- detector geometry used by Tsai [1] and Tehranian [2]. These experiments were conducted by vaporizing chromium disks masked by tantalum foil with spark-cut apertures between 1 and 9.5 mm diameter. The masked samples were held in a molybdenum sample holder similar to one used for steady state calibration of the mass spectrometer. It was found [17] that increasing the aperture radius, up to a limiting value R_m , increased the mass spectrometer signal for the target held at a fixed temperature. For aperture radius larger than R_m , no further increase in the signal was observed. The experimental data were used to fit two adjustable parameters in an assumed mathematical form of w(r) in Ref [17].

The effect of the collimator function on the mass spectrometer signal during laser pulsing is also considered in Ref [17]. The theoretical expression for number density n(t) is derived accounting for the contributions from various radial locations on the heated target. This results in a modified version of Eq. (2.3). Tsai's data [1] were reevaluated with the experimentally determined w(r) in the revised Eq (2.3). However, the discrepancy in inferred vapor pressure could not be resolved.

In the present investigation, the target- collimator- detector geometry was altered from the one previously used [1,2] to increase mass spectrometer sensitivity. The new geometry is shown in Fig 5.5. The collimator efficiency was determined by the method described above. Fig 5.6 shows the measured mass spectrometer signals as a function of temperature of a uniformly heated chromium samples masked to give different aperture radii. As observed previously [17], the mass spectrometer signal increases with aperture radius for a fixed temperature. However, the limiting radius R_m that existed in the previously-used geometry could not be observed in the new geometry *even* when the aperture radius was made equal to the target diameter. This shows that the collimator efficiency is strongly dependent on the target- collimator- detector geometry.

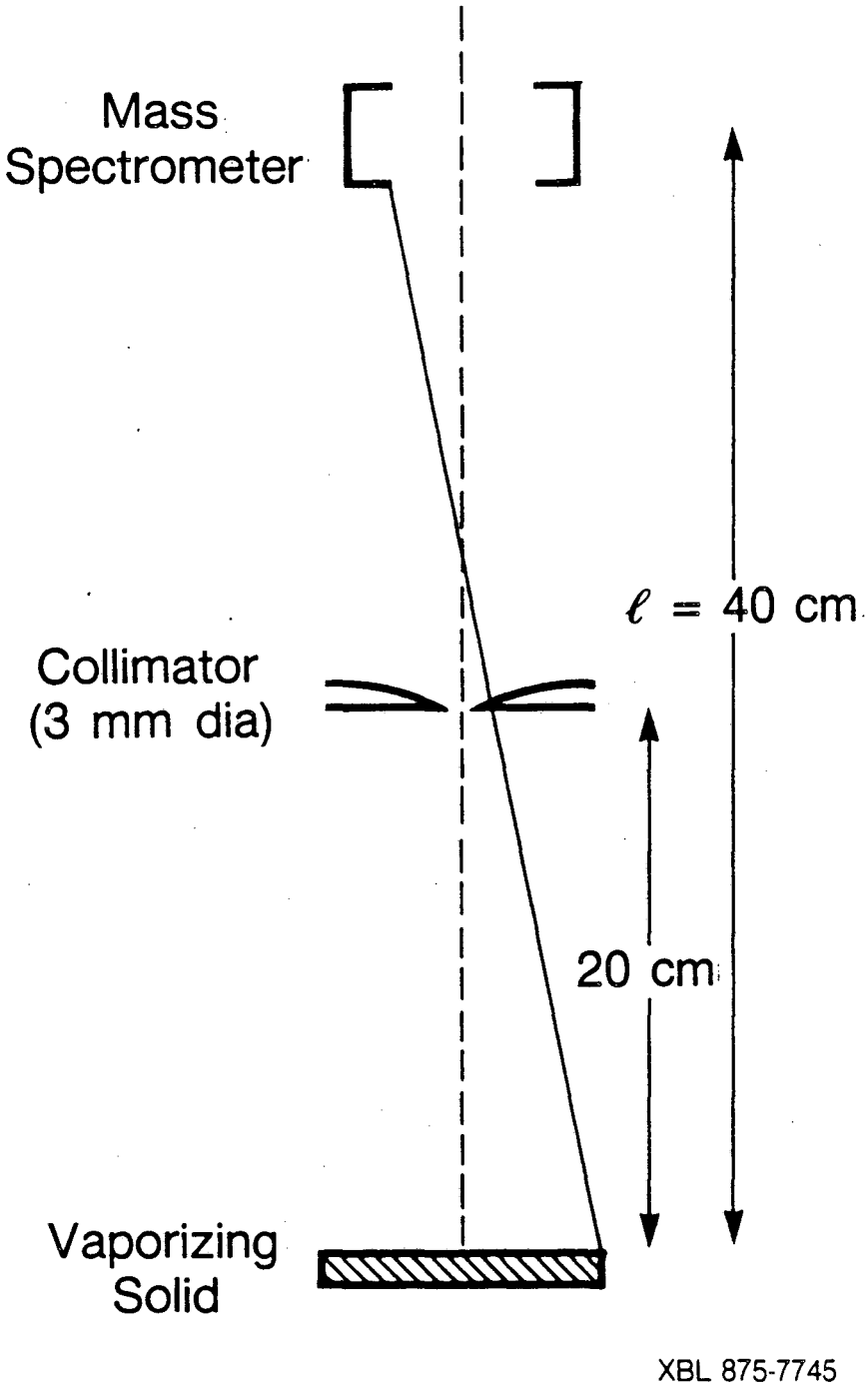
Mass
Spectrometer
ℓ = 40 cm
Collimator
(3 mm dia)
20 cm
Vaporizing
Solid
XBL 875-7745

Fig. 5.5

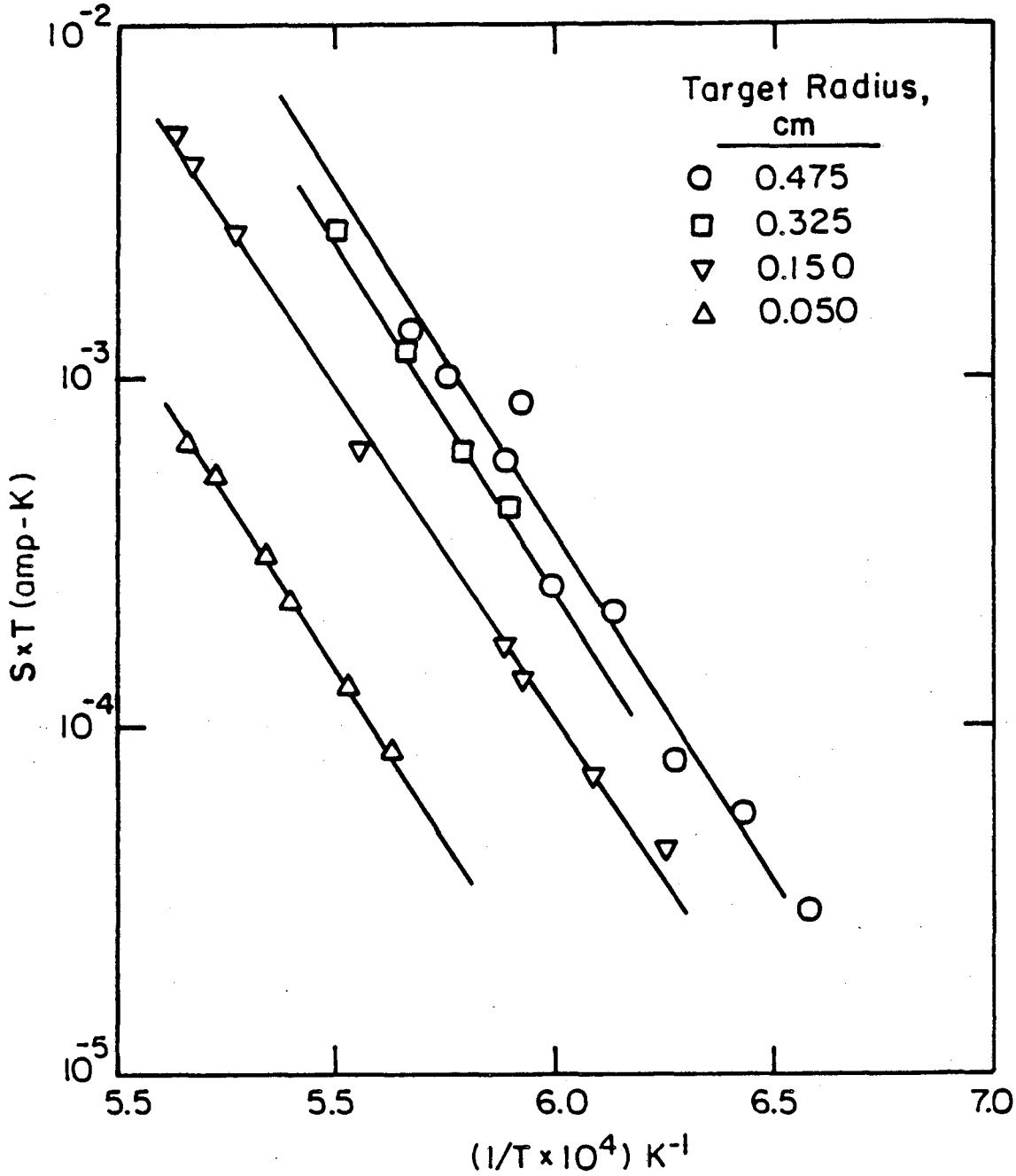

XBL 861-7441

Fig. 5.6

For the geometry shown in Fig 5.5, the collimator efficiency was assumed to have the following form:

$$w(r) = C\, e^{-ar^2} + (1-C)\, e^{-br^2} \tag{5.1}$$

where C,a,b are adjustable parameters. Fitting the experimental data points of Fig 5.6 to Eq (5.1) resulted in C = 0.9594, a = 7.4457 and b = 0.9625. In Fig 5.7 experimental w(r) is plotted and compared with the one based on assumption used in Ref [1] and [2].

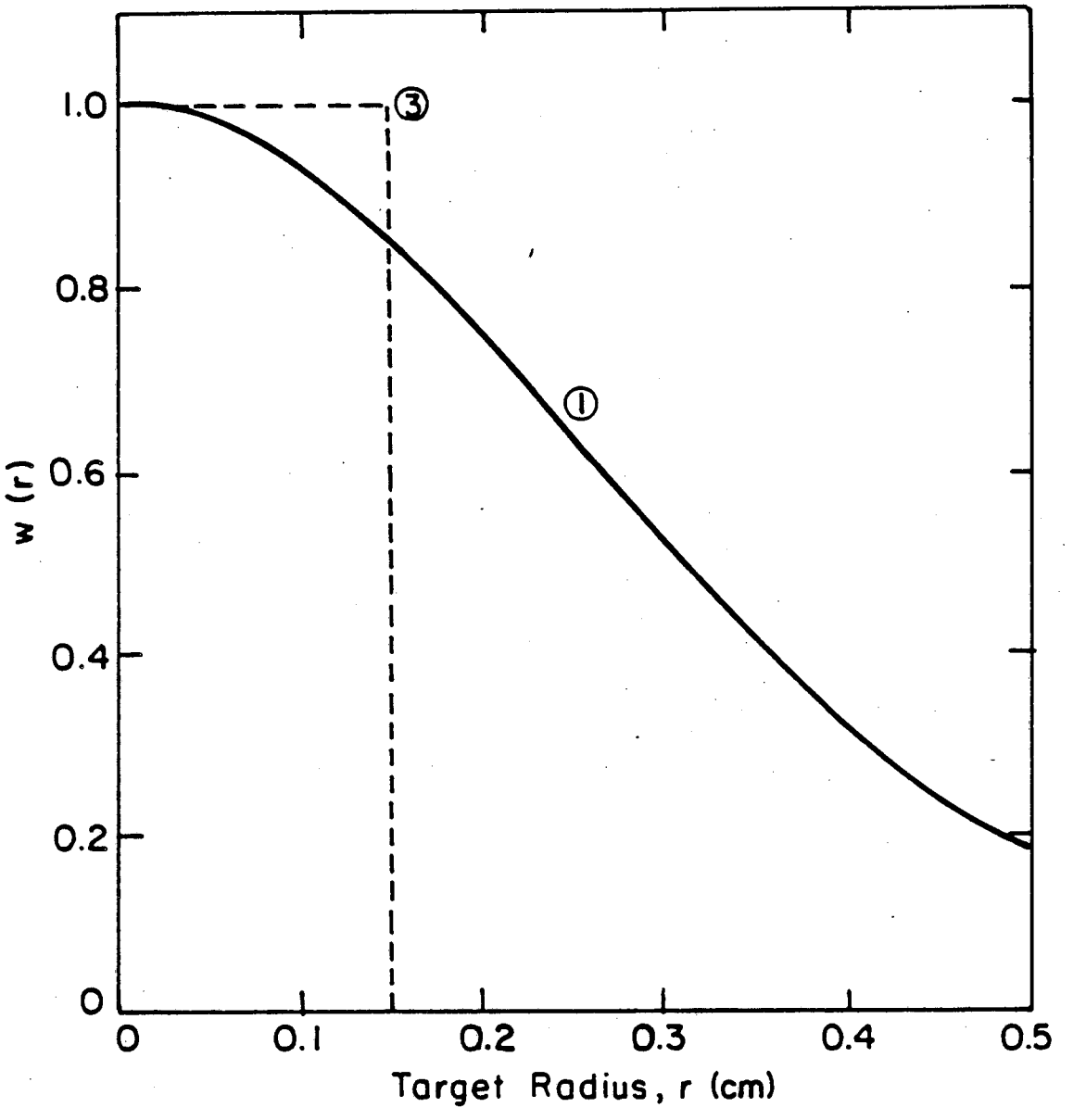
1.0
0.8
0.6
0.4
0.2
0
w (r)
0
0.1
0.2
0.3
0.4
0.5
Target Radius, r (cm)
③
①
XBL 861-7447A

Fig. 5.7

CHAPTER 6

RESULTS

1. MASS SPECTROMETER CALIBRATION

The mass spectrometer was calibrated by two separate methods. The first method of heating of UO_2 specimen to known steady temperatures below melting point was identical to the one used in Ref [1] and [2]. The second method involved low intensity laser pulse heating of UO_2 target, in the manner similar to the one intended to be used for vapor pressure measurements, except for the lower surface temperatures.

1.1. Stoichiometric Specimens

The specimens used for the calibration were cut from pellets of nominally stoichiometric UO_2 and were used without any polishing.

1.1.1. Steady State Method

For steady state calibration of the mass spectrometer, method identical to the one used in Ref [1] was employed. Specimens (1 cm diameter and 1 mm thick) were cut from nominally stoichiometric UO_2 pellets. The current signal, I, for UO_2 , UO, U and UO_3 obtained from the mass spectrometer as a function of target surface temperature T are plotted in standard format in Fig 6.1. The slopes of the lines in Fig 6.1 give the heat of vaporization ΔH_{vap} for different uranium bearing species. ΔH_{vap} values of 141 ± 13, 137 ± 8, 141 ± 10 and 153 ± 16 kcal/mole were obtained for UO_2 , UO, U and UO_3 respectively. The error limits on these values are for 95 % confidence. These values are in good agreement with those reported in [1].

The measured mass spectrometric signals for each of the uranium-bearing species has contributions from the fragmentation of heavier species in the ionizer. The fragmentation pattern can be computed from the data on Fig 6.1. One method of this computation is given in Refs [1,2]. Finally, the mass spectrometer calibration constants for each of

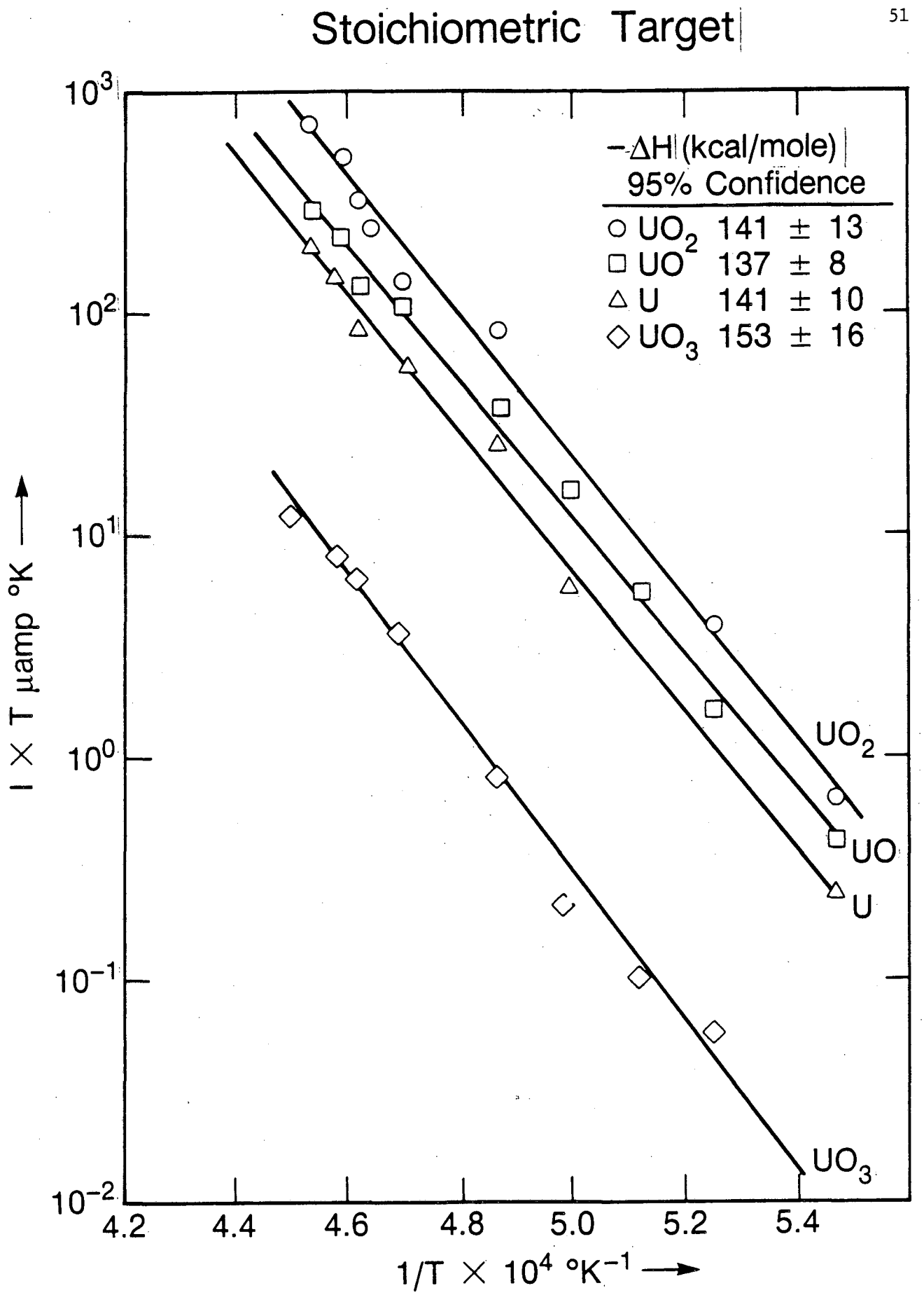

Fig. 6.1

XBL 876-7762

the species can be obtained from the knowledge of the fragmentation pattern and the low temperature partial pressures.

1.1.2. Transient Method

Unfocused laser pulses of low energy irradiated UO_2 target surface so as not to exceed the melting point. Target surface temperature transient and the output from the mass spectrometer for each of the four uranium bearing species were monitored.

A complete analysis of the transient calibration data would require the use of the modified version of Eq (2.3) that includes collimator efficiency function w(r), and the fragmentation pattern (section 1.1.1 of this Chapter). Such an equation would yield calibration constant $K_{MS}\sigma\gamma$ for each of the species with the knowledge of their partial pressures below melting point.

The consistency between the two methods of calibration of the mass spectrometer can be established by comparing the values of the calibration constants. A simple check for this would be to compare the strength of the UO_2 signals (which is the strongest among the four uranium bearing species) from the two methods. Ignoring the fragmentation in the ionizer, the calibration constant, $K_{MS}\sigma\gamma$, for the steady state method is given by combining Eqs (2.1) and (2.2) :

$$(K_{MS}\sigma\gamma)_{ss} = \frac{I \times T}{K_g K_U P} \tag{6.1}$$

Using calibration data of Fig 6.1 for UO_2 signals for several different temperatures, an average value for $(K_{MS}\sigma\gamma)_{ss}$ can be estimated. Similarly, an approximate expression for the instrument calibration constant for the transient method is given by :

$$(K_{MS}\sigma\gamma)_{tr} = \frac{V(t)}{R_b\, n(t)} \tag{6.2}$$

where R_b is the input resistance of the waveform recorder, V(t) is the measured signal for UO_2 as a function of time with its maximum value V_{max} , and n(t) is the number density computed from Eq (2.3) with a maximum value of n_{max} . From measured V_{max} and computed n_{max} , an

approximate estimate can also be made for $(K_{MS}\sigma\gamma)_{tr}$.

The estimates of $(K_{MS}\sigma\gamma)_{ss}$ and $(K_{MS}\sigma\gamma)_{tr}$ thus obtained were compared. This comparison was satisfactorily consistent (within an order of magnitude) below a maximum surface temperature, T_{smax} ,of 2500 K. Above this temperature the mass spectrometer signals from the laser shots become inconsistent with respect to extrapolated steady state calibration.

In Fig 6.2 the maximum mass spectrometer signal measured for four different uranium bearing species, namely UO_2^+, UO^+, U^+, UO_3^+, is plotted as a function of maximum measured surface temperature. An unusual behavior is observed here. The magnitude of the signal first showed an increase with T_{smax} as expected but leveled-off as the temperature was increased. The slope of the rising part of the curves in Fig 6.2 is consistent with the steady state calibration factor of the mass spectrometer However, inconsistencies of up to two orders of magnitude are seen in the magnitude of the measured signal for the highest T_{smax} in Fig 6.2.

1.2. Hypostoichiometric Specimens

Since incongruent vaporization of UO_2 depends on the stoichiometry of the target, hypostoichiometric specimens were fabricated and used in the laser pulsing experiments. The following method was used for reduction of nominally stoichiometric UO_2 and determination of its stoichiometry.

Uranium dioxide pellets were reduced by contacting with small chunks of uranium metal and heating up to 1800 K for one hour in atmosphere of argon mixed with 5 % hydrogen. Subsequently, the stoichiometry was experimentally determined by measuring the weight gained by a sample from the reduced pellet upon air oxidation at low temperature.

To enhance proper contact between the oxide and the metal at high temperature for the reduction step, the metal chunks were placed inside a well drilled along the axis of the oxide pellet. The hole was drilled up to approximately two thirds of the oxide pellet height. After the

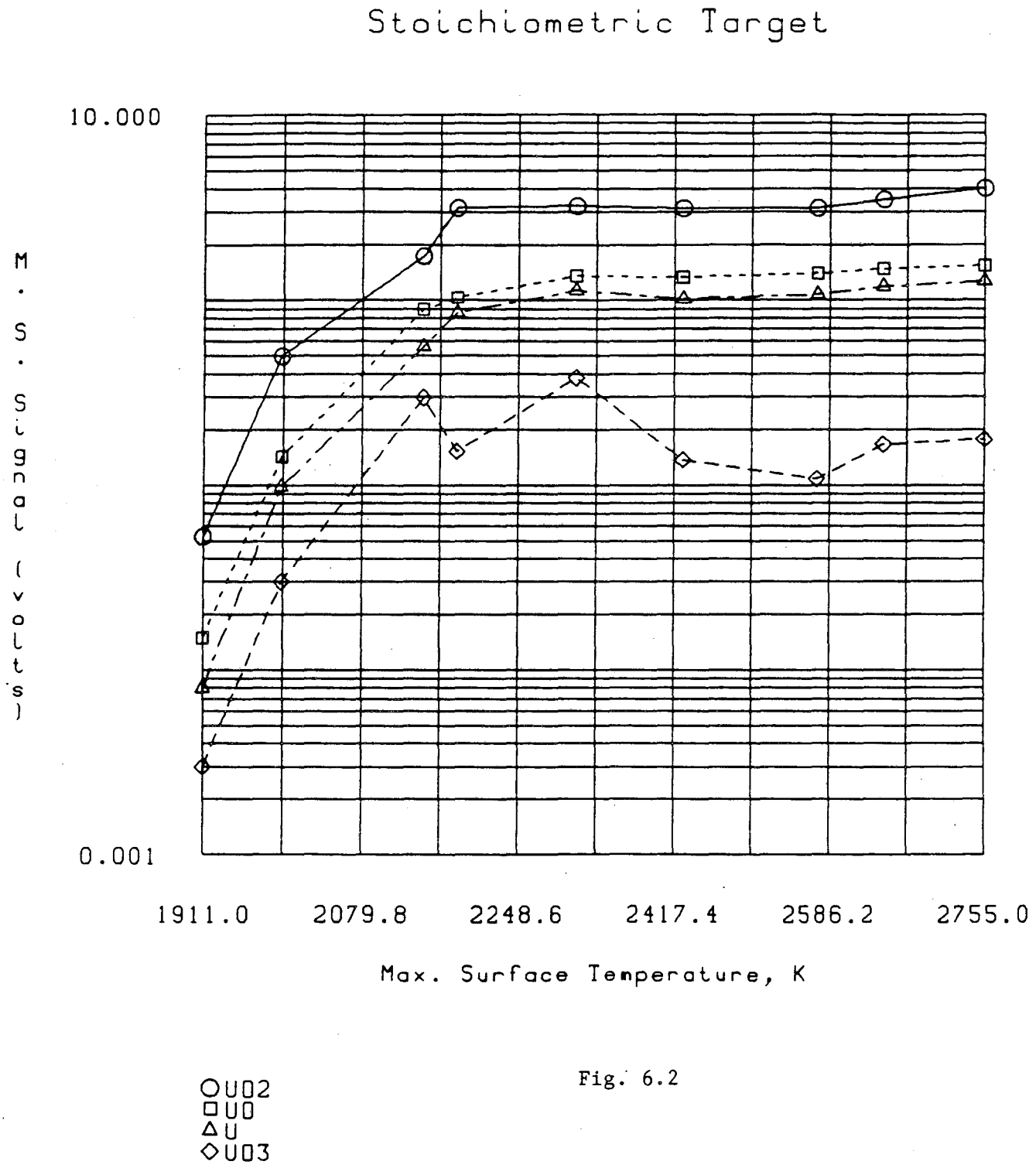
Stoichiometric Target
10.000
0.001
M. S. Signal (volts)
1911.0
2079.8
2248.6
2417.4
2586.2
2755.0
Max. Surface Temperature, K
UO2
UO
U
UO3

Fig. 6.2

reduction, the pellets were rapidly cooled in the inert gas mixture.

Target wafers were cut from the reduced pellets and were used in the laser pulsing experiments without polishing. However, several reduced wafers of urania were polished, etched and examined under an optical microscope. The micrographs showed evidence of metallic uranium phase in the oxide matrix; indicating that the reduction has indeed taken place.

The laser pulsing experiments detected all four uranium bearing species for the hypostoichiometric specimens. As shown in Fig 6.3, the magnitude of mass spectrometer signal showed a trend similar to the one observed for the stoichiometric targets.

It should be noted that due to possible changes in absolute sensitivity of the mass spectrometer, the magnitudes of the signals between Figs 6.2 & 6.3 are not directly comparable. Perhaps some useful thermochemical information can be obtained from the ratios of signals for various uranium bearing species. A comparison of these *ratios* from Figs 6.2 & 6.3 at a given T_{smax} may reflect stoichiometry dependent thermochemical data for UO_2 .

2. MASS SPECTROMETER SIGNALS

2.1. Temporal Shape

Figs 6.4 through 6.9 show the experimental mass spectrometer signals (traces directly from the recorder) for UO_2 for six laser shots of increasing power densities. The measured peak temperatures, T_{smax} , ranged from 2050 to 3400 K for these shots. Superimposed on these traces are the n(t) calculations, based on the free molecule vaporization where the recommended total pressures of UO_2 from Ref [7] were used. The number density calculations have been normalized to produce the same peak value as the signal traces.

Figs 6.4-6.7 (2059, 2235, 2430, 2435 K) show absolute agreement with the predictions for the shape of n(t) based on the free molecule vaporization; the time of arrival of the peak is nearly perfect and the

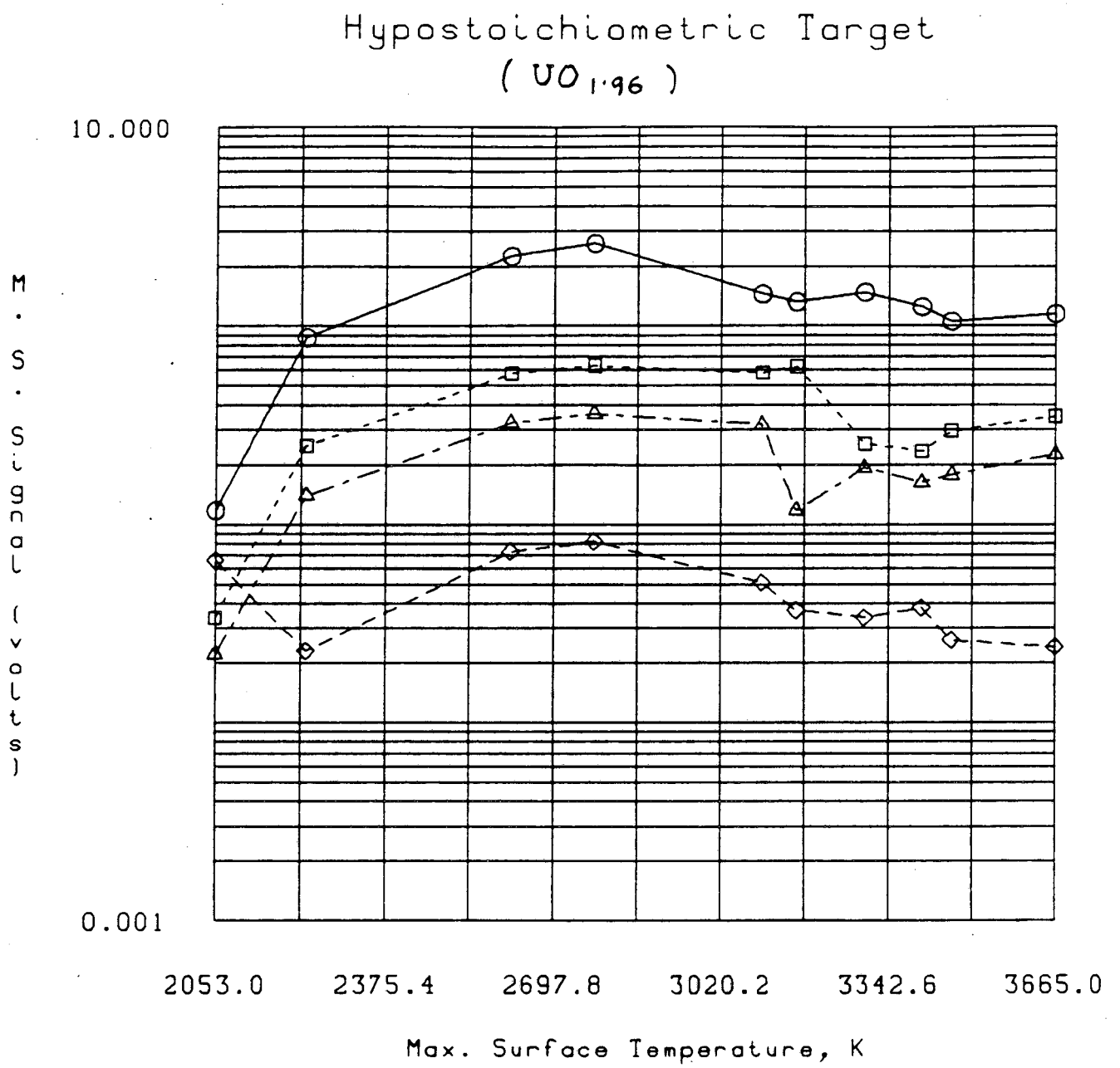

○ UO2
□ UO
△ U
◇ UO3

Fig. 6.3

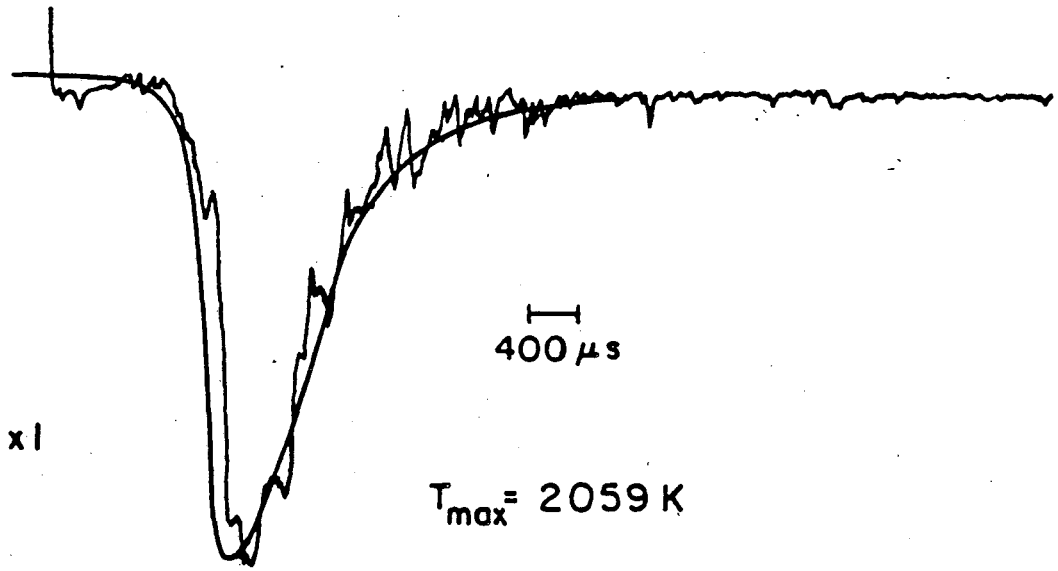

Fig. 6.4

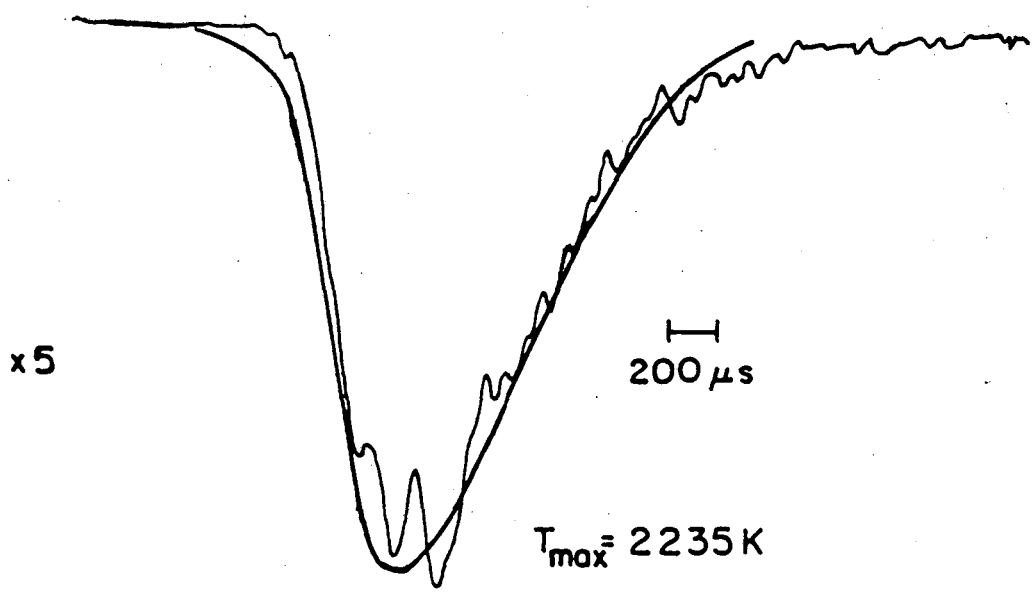

XBL 861-7444

Fig. 6.5

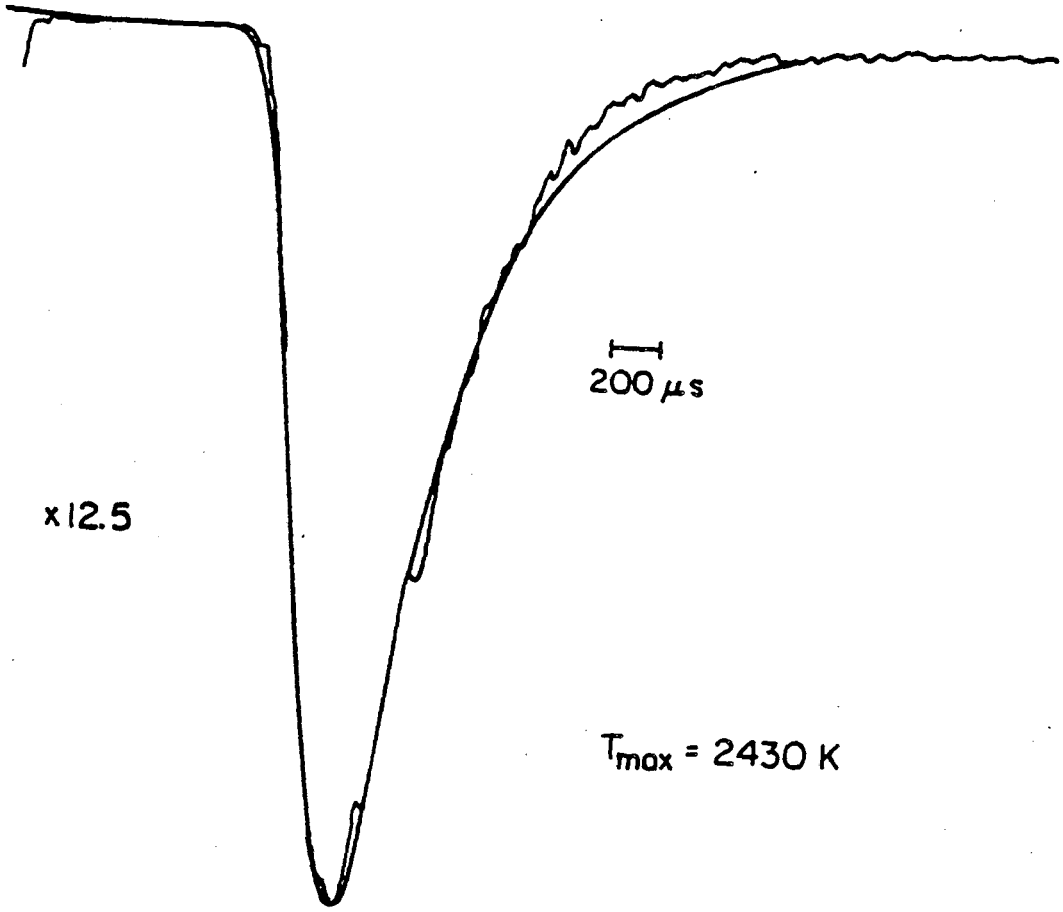

Fig. 6.6

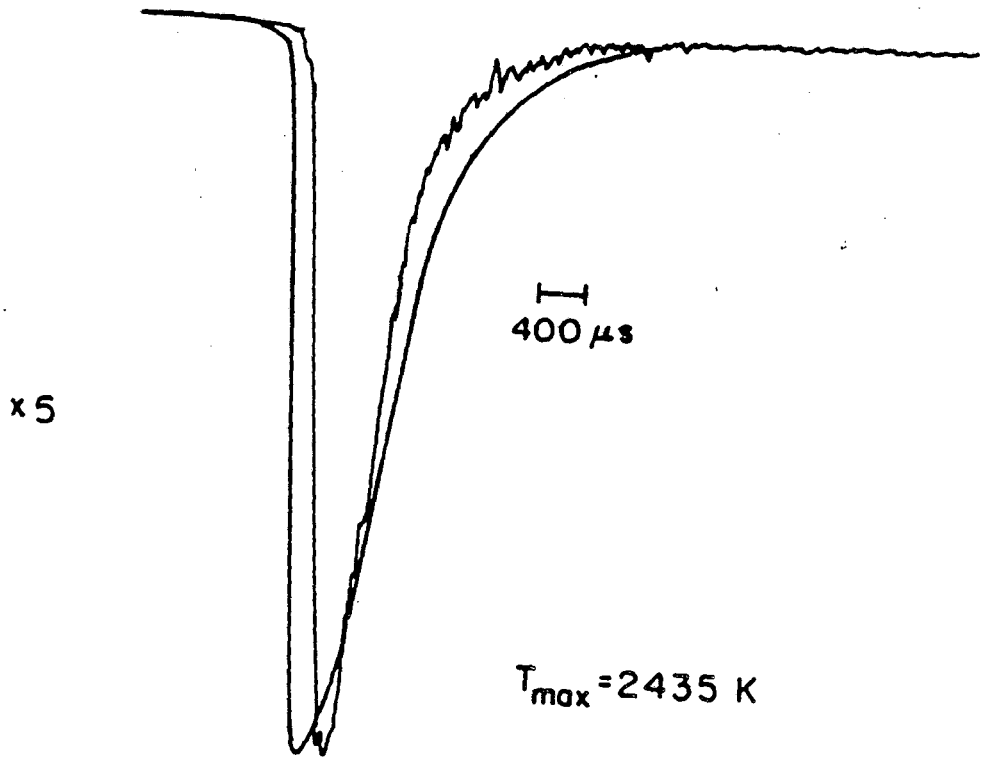

XBL861-7443

Fig. 6.7

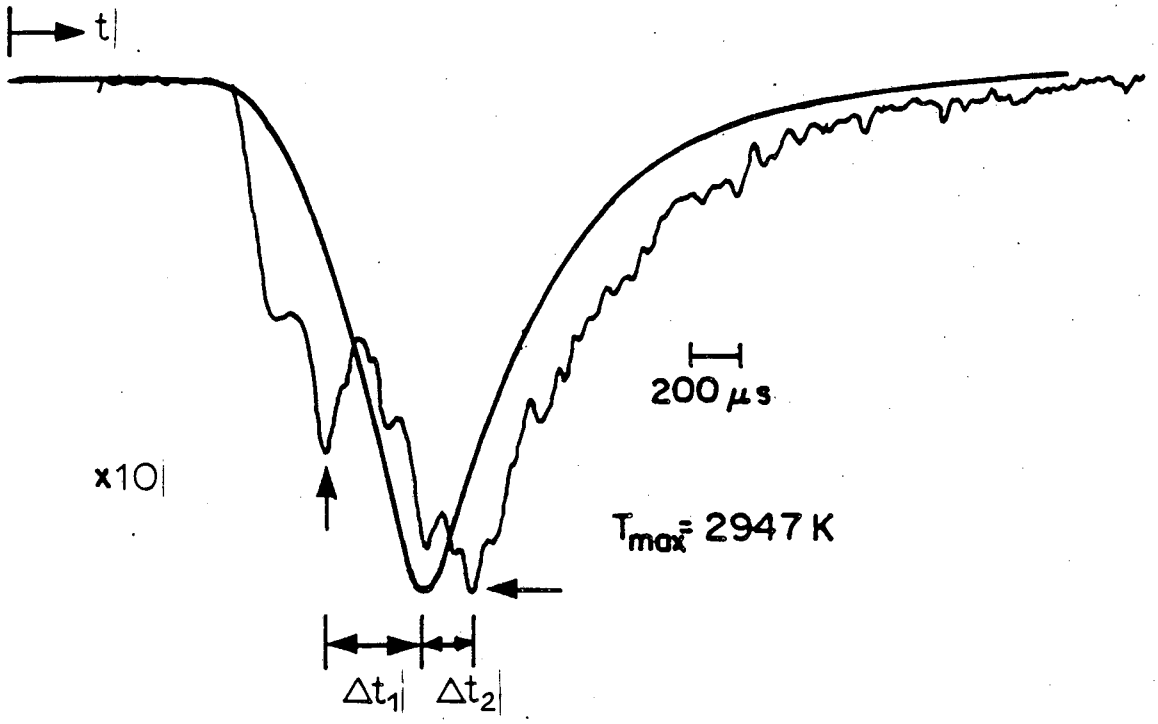
t
200 μs
x10
T_{max}= 2947 K
Δt_1
Δt_2

Fig. 6.8

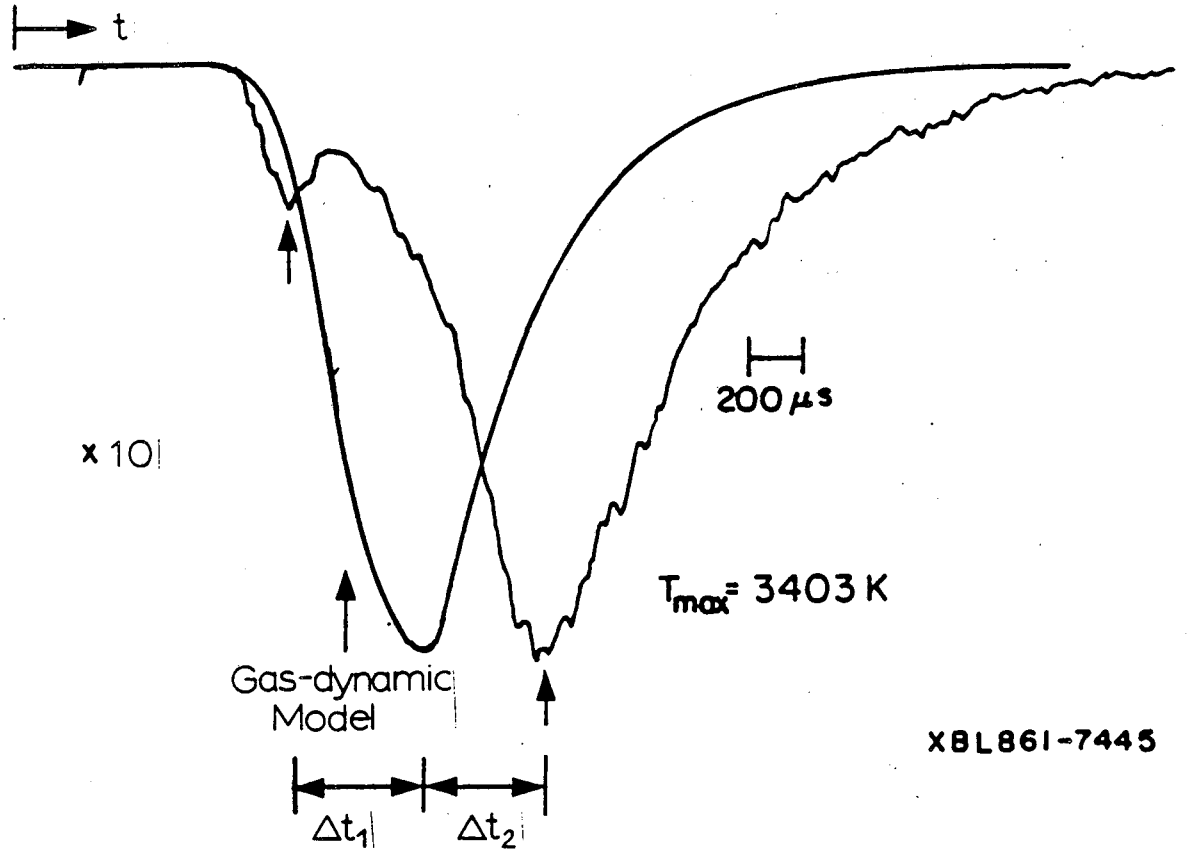
t
200 μs
x 10
T_{max}= 3403 K
Gas-dynamic
Model
Δt_1
Δt_2
XBL861-7445

Fig. 6.9

shapes of the experimental and theoretical curves agree well. The normalization factor (i.e. the calibration factor $K_{MS}\sigma\gamma$) is nearly the same for all these four shots. The normalization factor was also found to be in good agreement with the steady state calibration factor. A remarkable transition, however, is seen in Figs 6.8 & 6.9. The signal shape begins to distort with appearance of a "shoulder" on the rising part of the trace. As T_{smax} is further increased, the "shoulder" begins to appear like a distinct peak. The new peak (peak 2) occurs ahead of the predicted time for the maximum signal according to free molecule expansion and gas-dynamic expansion. At the same time, the maximum for the original peak (peak 1, which is distorted) occurs later in time. The time shifts Δt_1 and Δt_2 shown in Figs 6.8 & 6.9 increase with increase in T_{smax}.

For the latter two shots, three points are noteworthy. First, the experimental peak shifts to times greater than predicted for free molecule Hertz-Langmuir vaporization. Second, the fast peak (thought to be a fast ion peak in Ref [1]) begins to appear on the experimental traces. Third, the magnitude of the signal practically stops increasing with increase in T_{smax} . In Fig 6.9, the maximum peak signal is about a factor of 100 smaller than the expected value based on the four low temperature shots.

Similarly for other uranium bearing species (UO^+, U^+, UO_3^+) the temporal signals showed transition from a single peak to a two-peak trace.

2.2. Signal Magnitude

The peak value of the mass spectrometer signal for UO_2^+ is plotted against four different parameters in Fig 6.10. Two of the parameters, namely QP and T_{smax} , are experimentally determined whereas the other two, theoretical maximum number density and surface vapor pressure, are calculated ones. The range of steady state calibration (converted from current to volts to account for the different signal detection instruments used in the two types of tests) is also shown in Fig 6.10. For low temperature shots which gave good agreement in time of arrival for the peak as well as a constant normalization factor (i.e. Fig 6.4-6.7), the signal magnitude is higher (within a factor of 10) of the steady state

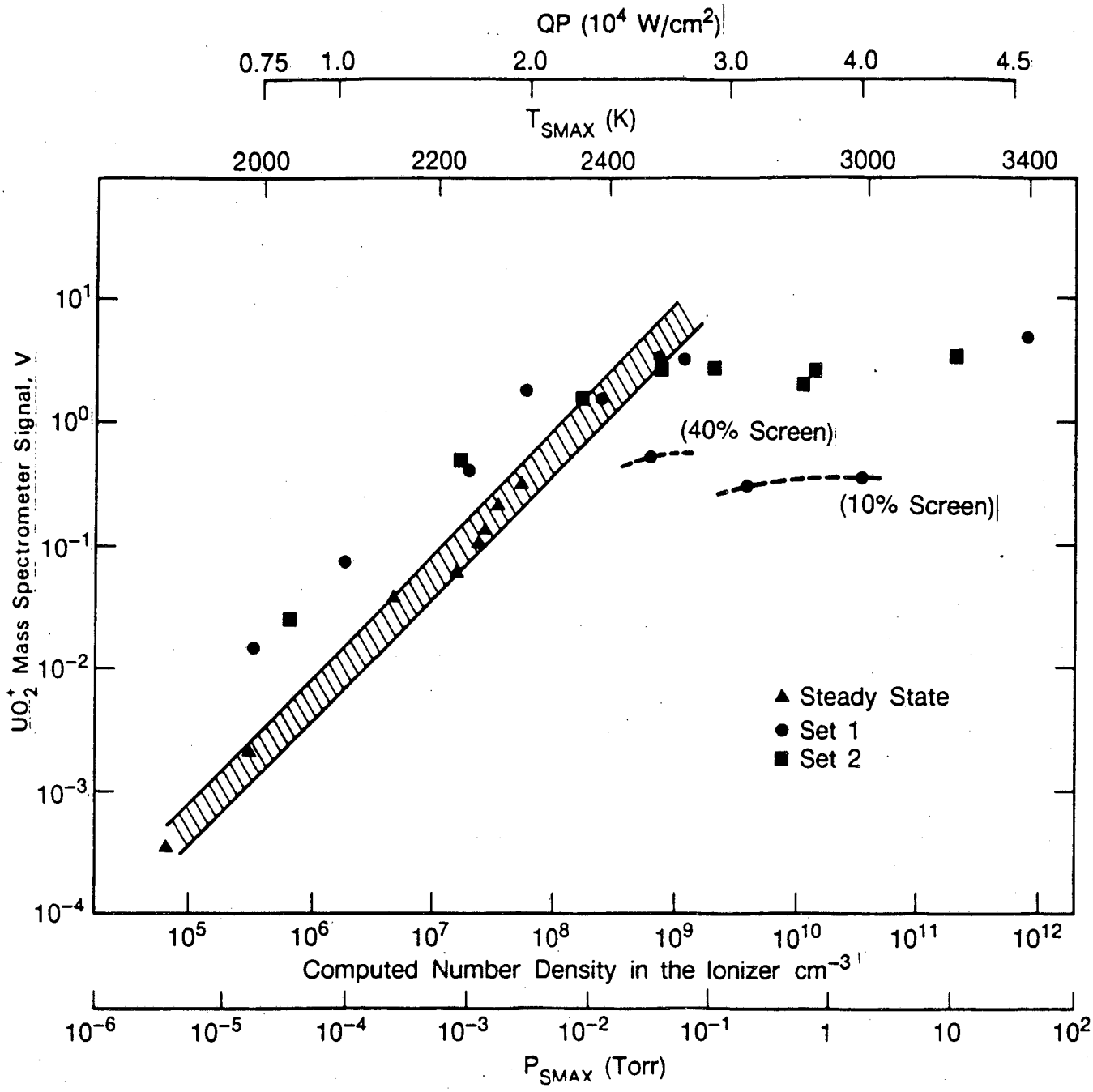
QP (10^4 W/cm^2)
0.75
1.0
2.0
3.0
4.0
4.5
T_{SMAX} (K)
2000
2200
2400
3000
3400
UO_2^+ Mass Spectrometer Signal, V
10^1
10^0
10^{-1}
10^{-2}
10^{-3}
10^{-4}
(40% Screen)
(10% Screen)
▲ Steady State
● Set 1
■ Set 2
10^5
10^6
10^7
10^8
10^9
10^{10}
10^{11}
10^{12}
Computed Number Density in the Ionizer cm^{-3}
10^{-6}
10^{-5}
10^{-4}
10^{-3}
10^{-2}
10^{-1}
1
10
10^2
P_{SMAX} (Torr)

Fig. 6.10

range. At higher T_{smax}, however, the signal is far lower than expected. It is clear from the data points of two different sets of laser pulsing experiments marked on Fig 6.10 that the magnitude of the mass spectrometer signal does not increase according to low temperature calibrations beyond T_{smax} of about 2500 K.

The mass spectrometer signal levels off precisely where the signals begin to show the time-of-arrival shift. The single point labeled "40 % screen" and two points labeled "10 % screen" were obtained by interposing screens of these transmissivity in front of the ionizer (section 1.1.1 of Chapter 5). The signal decreased by the expected amount indicating that mass spectrometer is responding linearly.

2.3. Comparison with Ref [1]

Tsai [1] did not observe consistent mass spectrometer signals for low temperature shots and the gradual transition to two-peaked signal trace, because his temperatures were above 2500 K for laser pulsing experiments.

3. IONIZATION OF THE EMITTED VAPOR

Laser irradiation is known to emit ions from the target material [9]. However, present experimental conditions did not favor ion generation because of the following reasons:

3.1. Low Laser Irradiance

The anomalous signal, which begins around T_{smax}=2500K, corresponds to a low laser irradiance of 5×10^4 watts / cm^2. Intrinsic ion generation with Q-switched, short pulsed lasers occurs at irradiance above 10^7 watts / cm^2 [9]. The present laser irradiance is nearly three orders of magnitude lower.

3.2. Thermodynamic State of the Vapor

Calculations of the thermodynamic state of UO_2 vapor reported by Karow [18,19] show that the degree of ionization in the vapor is rather low; it varies from 0.67 % at melting point (3130 K) to about 5 % at 5000 K. These estimates agree well with those of Ohse et al [4]. The latter also estimate the relative ion to neutral emission rates to be less than 13 % below 4000 K. But peak 2 appears at T_{smax} far below 4000 K, and is about 25% in peak height compared to peak 1 at T_{smax}=3400K .

3.3. Ion Detection and Deflection

Although the transition from one peak signal to two-peak signal in the present work occurs at rather low temperatures and irradiance conditions which do not favor ion generation, experimental attempts were made to detect any ions that may be present in the vapor and to deflect them prior to entering the ionizer of the mass spectrometer.

When the ionizer current of the mass spectrometer is turned off, both the peaks disappear from the signal trace indicating that neither is due to ions*.

If indeed ions were emitted from the target they will have to be high energy ions to be detected by the mass spectrometer since the ions will have to move up the ionizer cage potential (typically positive ten to fifteen volts above ground). Ions with such a high energy could only be present if the laser beam had intense hot-spots. However, the photographic technique used to measure the intensity distribution of the beam produced no evidence of such hot-spots. In addition, high energy ions, *if* present, would have very small detection efficiency in the cross beam configuration of the mass spectrometer used in this work.

---

*Tsai [1] reports to have observed ion peak with the ionizer current turned off. However, Tsai's laser beam was focused down to a spot size of 2 mm, unlike the unfocused beam used in the present work. Focusing of the laser beam gave nearly an order of magnitude higher laser heat fluxes in Tsai's work than those used in the present work as evidenced by higher T_{smax} in Tsai's work.

To test for the presence of the high energy ions, a second mass spectrometer was installed in an axial configuration for comparison with the cross beam configuration. However, no significant difference in the mass spectrometer response was observed. The phenomena similar to those described in section 2 were also observed with the axial mass spectrometer. If either of the peaks was due to ions, a strong signal from the axial mass spectrometer should have been detectable with its ionizer current turned off. Such a response, however, was not observed for unfocused beam.

Although the abundance of ions in the emitted vapor appeared to be low, they were deflected prior to entering the mass spectrometer chamber by application of sufficiently strong electric and magnetic fields. As shown in Fig 6.11, this was accomplished by application of sufficiently strong electric and(or) magnetic field. The electric field was in the form of d.c. potentials of opposite polarity applied to two circular metal screens placed parallel to the target. The screens were respectively 8 and 16 cm away from the target. Both the polarities were applied to deflect positive ions as well as electrons. The latter could have been generated intrinsically from the target or from the impact of any high energy positive ions on the screen itself.

The magnetic field was created using two SmCo rectangular permanent magnets. The magnets, each 5 x 2.5 x 1.25 cm in size, were held apart using metallic stand-offs such that the magnetic field lines were perpendicular to the axis of the collimator. The flux density (measured to be 0.07 to 0.10 T between the magnets) was sufficiently strong to deflect charged particles anticipated in the emitted vapor.

The trend in the mass spectrometer signals did not alter with application of either the electric or the magnetic fields or both. The gradual level-off of the magnitude and the transition from one-peak signal to two-peak signals was still observed. This proves conclusively that the fast peak in Figs 6.8 & 6.9 is not due to ions.

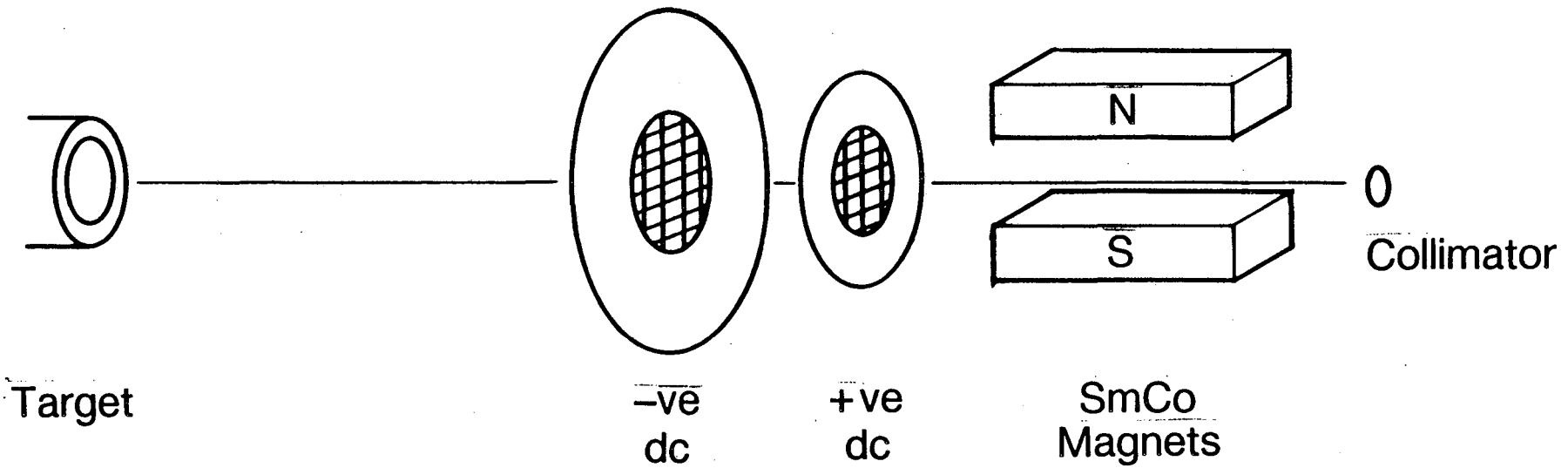

XBL 875-7746

Fig. 6.11

4. TARGETS OTHER THAN UO_2

To see whether the observed trend in the mass spectrometer signals has its origins in the nature of the target material itself, two other target materials were chosen for laser pulsing experiments. These materials were chromium and high purity stabilized zirconia. Chromium represents monatomic metallic species having properties quite different from UO_2, whereas zirconia is a refractory oxide which presumably has vaporization characteristics similar to that of UO_2. This was indeed confirmed by the laser pulsing experiments done on these materials. While the data for ZrO_2 were quite similar in trend compared to those of UO_2, chromium data were remarkably different.

High purity chips of chromium metal about 1.5 mm thick were spark-cut to 1 cm diameter wafers. The metal wafer was placed in the target holder instead of UO_2. The standard experimental procedure, described earlier in this report, for steady state calibration of mass spectrometer and transient laser pulsing was followed. The results are shown in Fig 6.12.

A clear overlap of steady state calibration data with the low QP laser shots is evident in Fig 6.12. For UO_2, the steady-state calibration line was nearly a factor of 10 lower compared to the calibration established by low-level laser pulsing. In addition, unlike UO_2 data, the magnitude of mass spectrometer signal for Cr^+ does not tend to level-off for high surface temperatures. (Similar behavior was observed by Olstad [20] for iron, another monatomic metallic target material.) The magnitude of Cr^+ signal for high QP laser shot remains consistent with the extrapolated values of the steady calibration data. Finally, the temporal shape of the signal trace had only one peak present. The transition from one-peaked to two-peaked signal (which was observed well below the melting point for UO_2) was not observed nearly up to the melting point for chromium.

When a target specimen machined from high purity stabilized zirconia was used in the experiments, the magnitude of the signal ceased to increase with increasing QP and, therefore, with increasing T_{smax}.

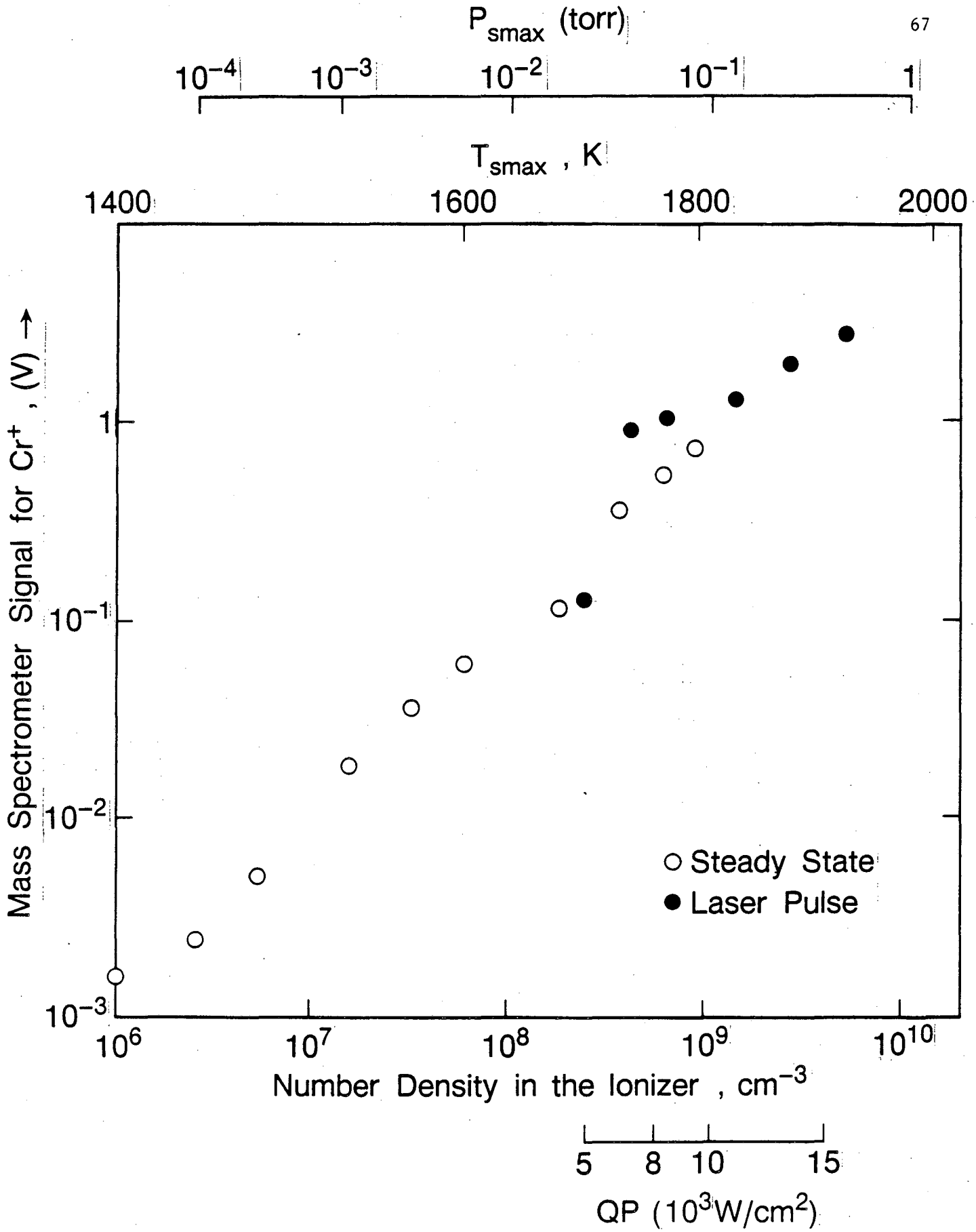
P_{smax} (torr)
10^{-4}
10^{-3}
10^{-2}
10^{-1}
1
T_{smax} , K
1400
1600
1800
2000
Mass Spectrometer Signal for Cr^+ , (V) →
1
10^{-1}
10^{-2}
10^{-3}
Steady State
Laser Pulse
10^6
10^7
10^8
10^9
10^{10}
Number Density in the Ionizer , cm^{-3}
5
8
10
15
QP ($10^3 W/cm^2$)

Fig. 6.12

Also unlike chromium the temporal shapes of the mass spectrometer signals showed *two* peaks. A comparison of laser pulsing data for chromium and ZrO_2 target is given in Fig 6.13. Since pressure of a given species at the target surface ultimately governs the magnitude of the mass spectrometer signal, it is illustrative to compare this parameter for chromium, zirconia and uranium dioxide data. For the data shown in Fig 6.13, the vapor pressure corresponding to the lowest and the highest temperature laser shots ranged from 1.5×10^{-2} to 6.0×10^{-1} torr for chromium and 7.5×10^{-6} to 1.0×10^{-2} torr for zirconia. For UO_2, the peculiar mass spectrometer response (leveling-off of signal magnitude and appearance of the second peak) occurred at surface pressure of about 5×10^{-2} torr. It is evident from these numbers that mass spectrometer *does* respond in accordance with the steady state calibration data for chromium at surface pressures at least up to an order of magnitude larger than it does for the oxides.

5. SURFACE HEATING RATES

The rate of surface heating is believed to be a parameter of great importance in vaporization kinetics. Breitung and Reil [21] have discussed that equilibrium vaporization may not occur at extremely rapid surface heating rates because undesirable phenomena such as explosive ejection of target material may be taking place. Also, these high heating rates are known to give superheated liquid layers on target surface. In the work of Bober and Singer [15], stainless steel heated at 3000 K/ms by a laser irradiance of 10^6 W / cm^2 gave superheated liquid layer on the surface resulting in a factor of two *reduction* in measured vapor pressure at 4000 K. It has been suggested in Ref [15] that the heating rates should be kept below 500 K/ms at melting point to keep evaporation close to equilibrium.

Since the present laser system delivered a fixed pulse width (except for a slight variation around 1 ms depending on the charge-up of the power supply), the heating rates of target could not be varied. Estimates of the heating rates of the target surface based on approximating the measured temperature transients by a triangular shape varied from 400 K/ms to 3100 K/ms for laser shots resulting in T_{smax} of 1800 K and 3150

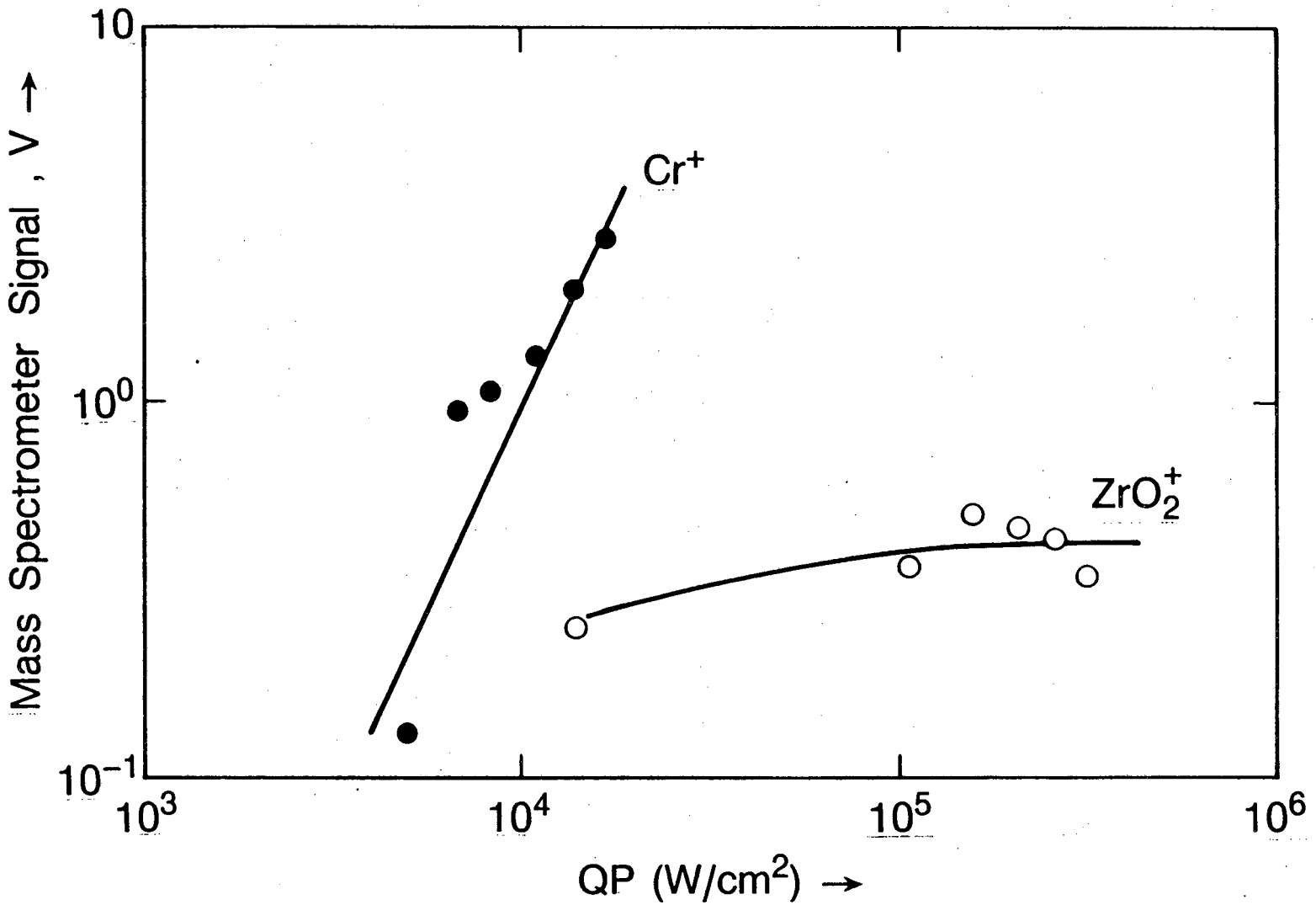

XBL 875-7741

Fig. 6.13

K respectively. Despite such high heating rates, non-equilibrium vaporization is not believed to be the cause of the peculiarities of the mass spectrometer response discussed earlier. This is because of the following reasons :

First, the inconsistencies in the mass spectrometer signals begin to occur *below* the melting point of UO_2. The phenomena causing non-equilibrium vaporization as put forth in Refs [15] and [21], namely the explosive ejection of liquid droplets and superheating of liquid layer at target surface, apply to temperatures above the melting point. Second, transient calibration data plotted in Fig. 6.10 suggests that for T_{smax} below melting point of UO_2, the transient signals are larger in magnitude compared to the steady state signals. Therefore, non-equilibrium effects, if any, would yield higher-than-expected signals, not lower ones for temperatures above the melting point.

Finally, a series of tests done with a much larger laser pulse width showed no remakable change in the trend of mass spectrometer signals. By modifying the capacitance and inductance of laser system's power supply, the manufacturer altered the laser pulse width from 0.75 ms to 1.75 ms. A series of laser pulsing experiments were performed with the modified laser. The increased pulse width gave nearly three times lower surface heat-up rates. Estimates similar to the ones stated earlier now ranged from 250 K/ms at T_{smax} = 1850 K to 1410 K/ms at T_{smax} = 3150 K. The gradual initial increase in the magnitude of the measured mass spectrometer signal with temperature and eventual level-off at high T_{smax} was also observed in this test series.

6. NEUTRON ACTIVATION ANALYSIS

In view of the observed anomaly in the mass spectrometric measurements, it was decided to use an alternate method [22] to determine the amount of UO_2 vaporized. For this purpose high purity graphite collector was placed in the pathway of the laser blow-off. Thus the vaporized species would simply deposit on it. Subsequently neutron activation analysis was used to determine the total amount of vaporization.

The target-collector geometry is shown in Fig 6.14. Vapor blow-off from individual laser shots with T_{smax} between 2400 and 3700 K, were collected and the graphite collector for each shot was irradiated in a TRIGA research reactor together with a known uranium standard. A cooling period of 17 to 24 hrs following the irradiation was allowed for two reasons. Firstly, shorter cooling times would have given complex and rapidly changing gamma spectra due to short lived fission products. Secondly, the cooling time brings down the radiation exposure level during post irradiation handling and counting to an acceptable level. Following the cooling period, the Np^{239} photopeak at 278 keV was found to be suitably intense to provide good counting statistics. The overall accuracy of about 10 % for the amount of U collected was obtainable in this method. This method of monitoring the vaporization, of-course, has the disadvantage of losing information on the time-dependent evaporation rate and the identity of individual species vaporized, information which would otherwise be available on a mass spectrometer. However, the graphite disk traps all uranium-bearing molecules or even larger agglomerates that impinge on it.

To compute the total amount of U collected on the collector from the amount of UO_2 vaporized from the target, The Hertz-Langmuir equation with a unit evaporation coefficient was used. For T_{smax} above 2700 K a 18 % back scattering factor, which is based on detailed collision-dominated flow model [2], was applied. A geometric view factor for the parallel disc target-collector geometry was taken to be identical to the one used in radiative heat transfer.

Fig 6.15 shows the results from the neutron activation analyses. The figure shows the amount of uranium collected on the graphite collector plotted against inverse of T_{smax} , the measured target surface temperature. Also shown is the theoretically calculated amount of uranium on the collector based on the total vapor pressure equation [21,7] for UO_2 . The experimental data points are in good agreement with the theory at high T_{smax}. The measured amount, however, is larger compared to the theory below melting point. It is possible that this discrepancy is connected to a similar discrepancy between the steady-state calibration line for UO_2 and the calibration established by low-level laser pulsing as shown in

Target-Collector Geometry

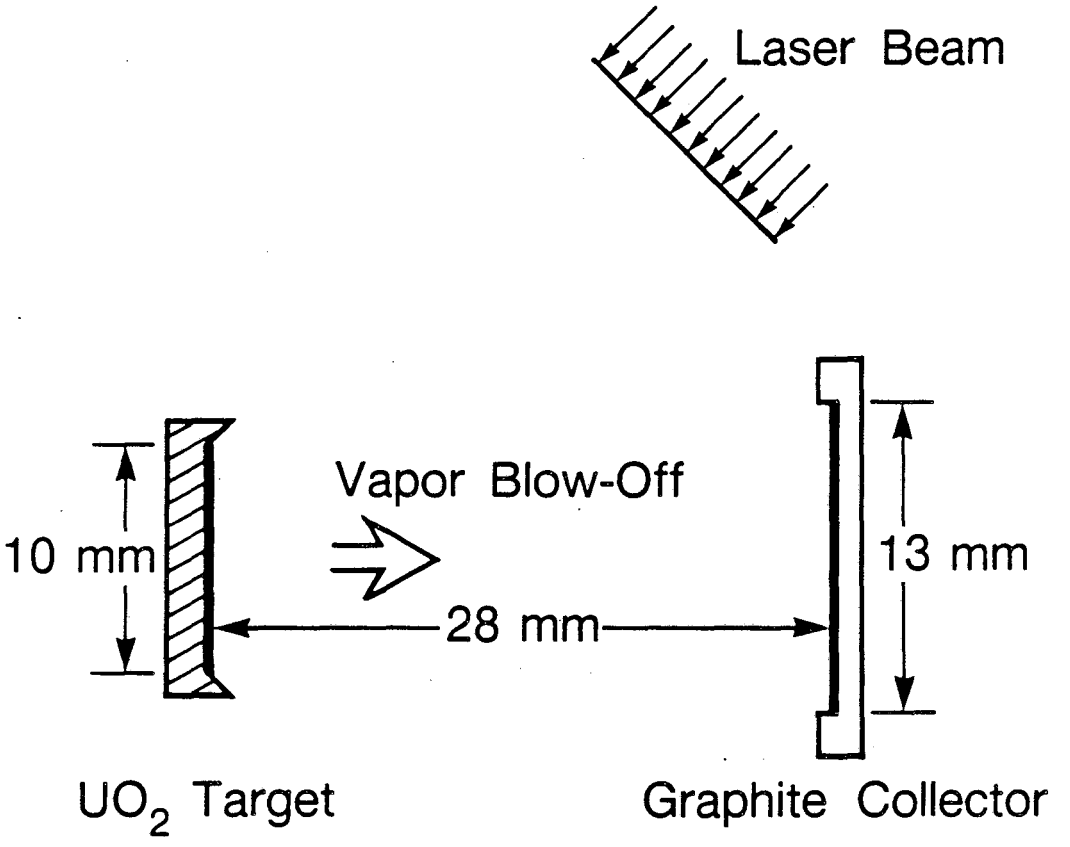

XBL 875-7744

Fig. 6.14

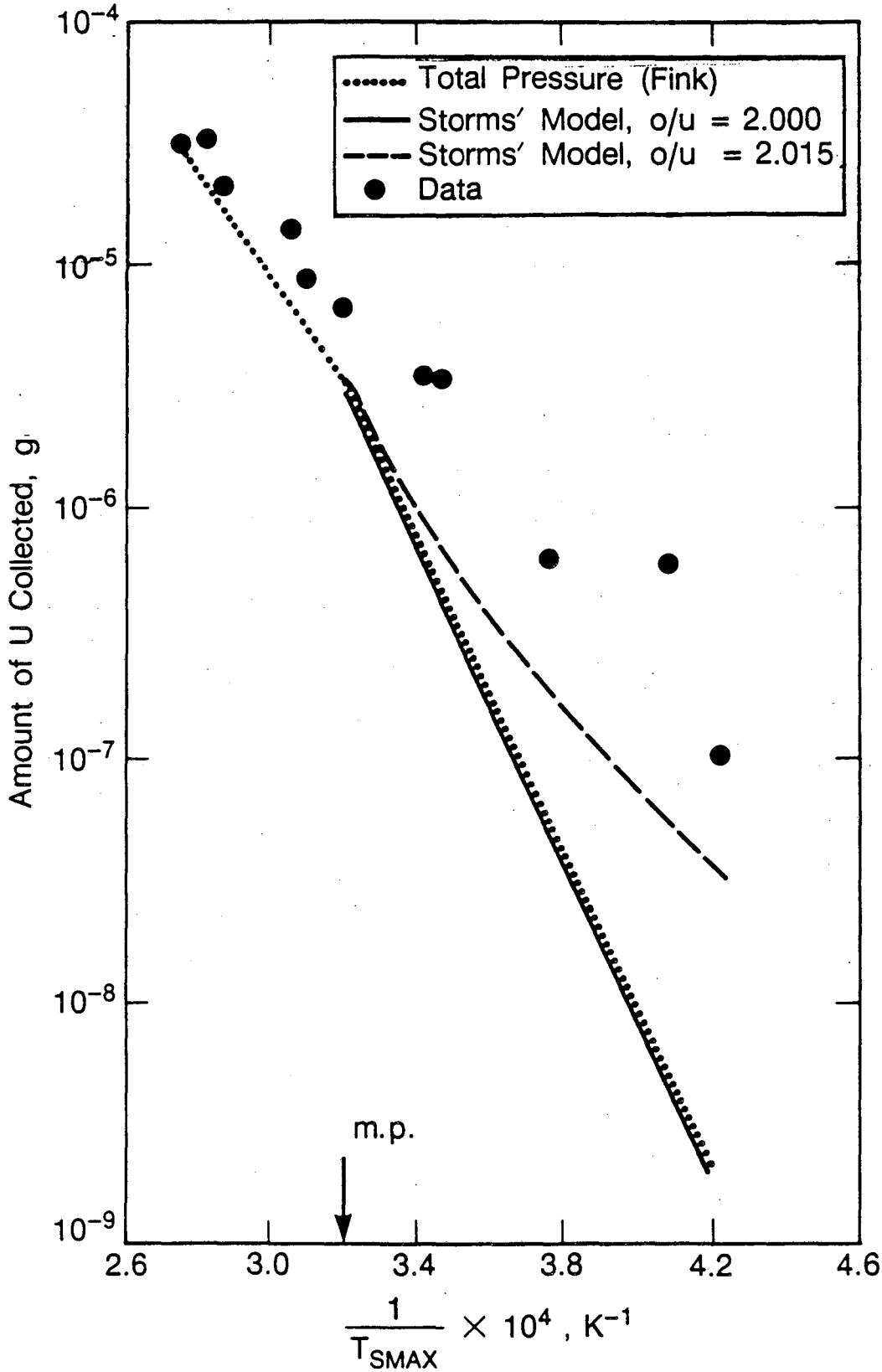

Fig. 6.15

XBL 874-7678

Fig. 6.10.

For the lowest T_{smax} shot, the amount of uranium collected is as much as 30 times larger than the amount expected. The discrepancy *decreases* with increase in T_{smax} . At least two possible reasons for the discrepancy can be speculated. Firstly, the stoichiometry of UO_2 affects the partial pressures of equilibrium gas phase species at a given temperature, especially that of UO_3 . Detailed thermochemical models proposed by Storms [23] and Green [24], predict larger partial pressures of UO_3 for hyperstoichiometric UO_2 than for stoichiometric UO_2. Although the target specimens were nominally stoichiometric, no specific attempt was made to control the stoichiometry in handling and preheating. It is possible that *even* nominally stoichiometric UO_2 target has highly hyperstoichiometric surface layers. For low T_{smax} , where only few surface layers are expected to vaporize, surface hyperstoichiometry and the consequent high volatility of UO_3 can contribute to greater amount of uranium collected.

To check on this hypothesis a simple test was performed. This test consisted of firing a strong pre-pulse on the target capable of vaporizing several μm of the surface. The purpose of this pre-pulse was to remove the surface layers which may be hyperstoichiometric prior to collecting vapor blow-off from a low temperature shot for neutron activation analysis. With the aid of a vacuum feed through, the collector was kept out of direct line of sight of the target during the pre-pulse. Immediately following the pre-pulse, the collector was placed in its usual position parallel to the target for collecting vapor blow-off from a low temperature laser shot. Subsequent neutron activation analysis, however, still showed that a *larger* than expected amount was collected in this test. Thus this test failed to confirm the hypothesis, however, the flaw in the test perhaps was that it took 42 seconds to position the collector in its proper place following the pre-pulse. This was the shortest time possible within the limitations of instrumentation and design. An estimate of rate of impingment of background water molecules on the target surface at 10^{-8} torr vacuum, showed that enough water molecules do strike the target surface within those 42 seconds to *reoxidize* the surface following the pre-pulse.

The second reason for the discrepancy is also based on the fact that for low T_{smax} shots the vaporization is limited only to few surface layers whereas for high T_{smax} shots vaporization from bulk* also occurs. The UO_2 target unirradiated by the laser shows surface pores and cracks as seen by scanning electron microscopy (Fig. 6.16). This rough surface would give surface area for vaporization which is much larger compared to the *geometric* target area alone. A larger surface area gives a larger amount of uranium on the collector. This additional contribution becomes increasingly *less* significant as T_{smax} increases.

*Assuming a uniform crater depth caused by the uniform laser intensity distribution, nearly 2 μ m of the target surface will vaporize for T_{smax} = 3600 K. However, for T_{smax} = 2400K only a fraction of a monolayer will vaporize.

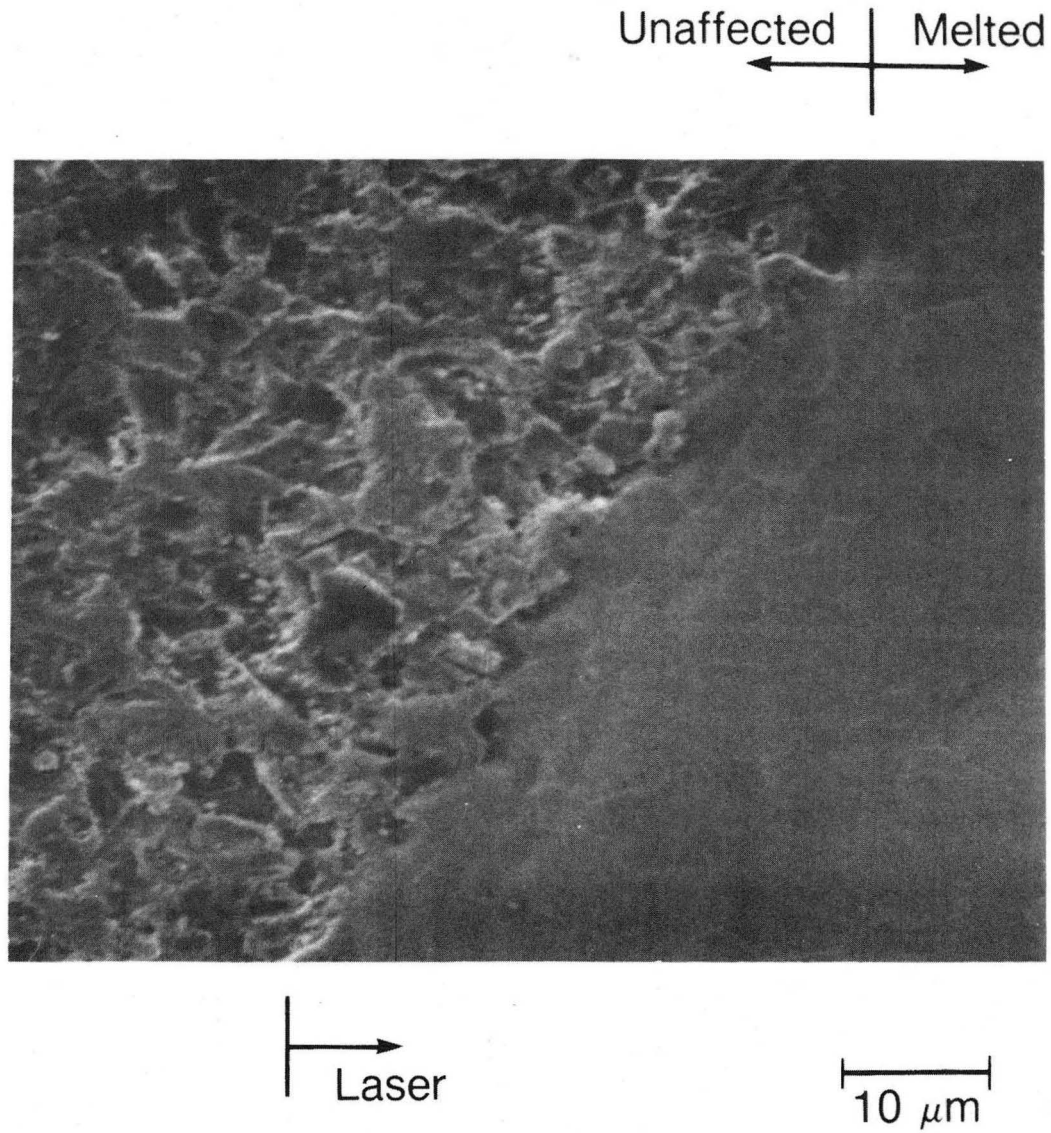

XBB 871-111

Fig. 6.16

CHAPTER 7

DISCUSSION

1. BACKGROUND

The experimental results and series of tests performed to understand mass spectrometer's response and to characterize the nature of laser-induced vaporization of UO_2 were described in Chapters 5 and 6.

For the high T_{smax} attained by the laser pulsing of the target, an output of large magnitude from the mass spectrometer is expected if the steady state calibration data were to be linearly extrapolated. Based on the data shown in Fig 6.10, a maximum output of nearly 100 volts is expected at T_{smax}=3200K. The instrument is incapable of delivering such large signals mainly because of the current drawing limitations of its electron multiplier. A careful examination of mass spectrometer signal showed, however, that such an absolute saturation of the instrument does not occur because it would have appeared as a flat top segment on the signal trace. Moreover, the instrument was found to respond linearly for the surface temperature range investigated for UO_2 and other solids during laser pulsing.

Ionization of the emitted vapor and the rate of surface heating proved to play no direct role in the observed mass spectrometer response. A trend in experimental data similar to UO_2 occurred with another oxide (ZrO_2); but not with element Cr.

In the mass spectrometric measurements, the agreement between the theory and the experimental data existed at low temperatures. On the other hand, the neutron activation analysis results showed good agreement with theory for high temperature pulses. It is believed that the reasons for the agreements and the discrepancies occurring in different temperature ranges in two independent methods of measurements are unrelated and not due to any instrument malfunction or measurement errors.

These observations point to the fact that simple free molecule model for the vaporization is not a valid one for the entire range of T_{smax} investigated.

2. INTERPRETATIONS

2.1. Validity of Free Molecule Flow

The theoretical model assumes that laser vaporized UO_2 from the target constitutes free molecule flow. A good agreement between the theory and experimental data below 2500 K proves validity of this assumption. However, gas phase collisions, reactions and condensation are neglected in the theory. As T_{smax} is increased the collisions in the gas phase are likely to become frequent and the vapor expansion can not be strictly modeled by free molecule flow. Tehranian [2] developed a gas dynamic vapor expansion model for laser-driven vaporization. Since collisional flow tends to speed-up the time-of-flight to the ionizer, the maximum number density at the ionizer of the mass spectrometer according to this model occurs earlier than that for free molecular flow. This expected time for peak signal is also shown in Fig 6.9 for comparison. It falls between peak 1 and 2 of the recorded mass spectrometer output.

Tsai and Olander [25] have examined transition from free-molecule to collision-dominated flow from vaporizing targets under several conditions of heating. Their results indicate that the transition must occur for T_{smax} around 2700 K for pulse heating. This temperature roughly agrees to the T_{smax} where observed deviations in the measured signals began (Fig 6.10). Despite this agreement, the collision dominated flow model can not explain the mass spectrometer's response with two peaks and the mismatch in the time for maximum signal.

2.2. Condensation of Vapor Blow-off

Laser pulse vaporization has often been compared to free-jet expansion from an orifice. Covington et. al. [14] used a photographic methods to show that laser pulse heating of graphite gives vapor blow-off similar

in structure to gas flows through orifice. The flow-pressure relationships in orifice flow were also found to be valid in the laser pulse blow-off. In such cases the bulk speed of the expanding vapor-jets may exceed local speed of sound. Since supersonic expansion of a gas through orifice causes considerable cooling in the flowing gas, it is also likely that the laser-driven vapor-jet will cool and condense. The condensation may form polymer species (such as dimers or trimers of UO_2) in the gas phase.

With the inclusion of gas phase condensation caused by supersonic expansion of the vapor-jet, it is possible to explain the anomalous mass spectrometer signal. The hypothesis is that peak 1 may be due to fragmentation * of the polymer species in the vapor. The fragmentation occurs as follows.

$$(UO_2)_n + e \rightarrow (UO_2)^+_{n-j} + (UO_2)_j + 2e$$

Due to their higher mass, the polymers have a longer time-of-flight to the ionizer. This fact is consistent with the observed delay in the time for maximum for peak 1. Peak 2, which occurs earlier in time compared to the free molecule flow model, may be due to monomers which arrived faster to the ionizer because of the collisional flow.

A model [26] based on free-jet expansion of UO_2 vapor in vacuum showed that substantial cooling indeed occurs. Provided that this supercooled vapor has sufficient time to nucleate and condense to polymeric species of UO_2 prior to its arrival at the ionizer of the mass spectrometer, the resulting signal from the mass spectrometer (which is tuned to detect the monomers only) may be masked.

The experimental evidence of this work that monatomic metallic species such as chromium do not show such masking of the signal (presumably due to condensation) is consistent with this hypothesis. When a dimer is formed to initiate the condensation process in the

* Ionizing electron energy was set at a rather high value of 70 eV for sensitivity reasons.

expanding vapor plume, the binding energy that is released is absorbed by internal degrees of freedom of the newly formed dimer. The dimer of a monatomic species such as chromium has a far fewer degrees of internal freedom (vibrational and rotational) compared to a dimer of a polyatomic species such as UO_2 or ZrO_2 . Thus the former tends to dissociate whereas the latter is stable.

If indeed polymers of UO_2 are formed in the vapor-jet, it is impossible to detect them by simple quadrupole mass spectrometer used in this work due to its limited mass range and poor sensitivity for high mass molecules. Other target materials such as chromium and ZrO_2 gave no measurable signals for dimers or trimers, possibly because of high degree of fragmentation by the 70 eV electrons in the ionizer.

Attempts to characterize the vapor blow-off were made by collecting it on a polished collector, placed close to the target while the latter is being pulsed by the laser. Subsequent microscopic examinations revealed a few liquid-like droplets (as opposed to a uniformly coated film) for laser shots where the maximum surface temperature exceeded the melting point of UO_2. The abundance of these droplets was found to be less than about 2%. The origin of these droplets may either be direct explosive ejection of liquid from the target surface or gas phase condensation. The latter may only result in these droplets *if* the degree of polymerization resulting from supersonic vapor jet expansion is high. Low degree of polymerization may still result in a uniform coat on the collector, and *not* the droplets. Tsai [1] also observed such droplets but concluded that their abundance (approximately 5%) was small enough to disregard substantial gas phase condensation to a high degree polymerization.

3. CONCLUSIONS

The magnitudes and temporal shapes of the observed mass spectrometer signals agree well with the free-molecule vacuum vaporization theory only at low surface temperatures. Possibly because of vapor-phase interactions, this agreement ceases to exist at temperatures above ~ 2600 K. Extensive experimental test proved that the this is neither

caused by ionization of emitted vapors nor by rapidity of surface heating. It was also thoroughly confirmed that extraneous factors such as instrument non-linearity or malfunction played no role.

The neutron activation analysis of the collected vapor blow off reveals that UO_2 *does* vaporize in accordance with its vapor pressure at temperatures above its melting point.

Some uncertainty in measured target surface temperature exists. However, computation and additional tests showed that the inaccuracies involved are not large enough to account for a nearly two orders of magnitude discrepancy in the mass spectrometer signals at temperatures above 3000 K.

It appears that the signal from the mass spectrometer is masked due to gas phase condensation. Therefore, the mass spectrometer signal can not be directly interpreted in terms of the vapor pressure of UO_2 .

REFERENCES

[1]
C. H. Tsai, " Kinetics of Laser Pulse Vaporization of Uranium Dioxide by Mass Spectrometry ", Ph. D. Thesis, University of California, Berkeley, LBL - 13679, (1981)

[2]
F. Tehranian, " Kinetics of Laser Pulse Vaporization of Uranium Carbide by Mass Spectrometry ", Ph. D. Thesis, University of California, Berkeley, LBL - 15982, (1983)

[3]
Ohse et. al., High Temp. Sci., 13 (1980) 35.

[4]
R. W. Ohse et. al., "Equation of State of Uranium Dioxide", J. Nucl. Mater., 130 (1985) 165.

[5]
M. Bober et. al., Nucl. Tech. 26 (1975) 237.

[6]
T.Yano, A. Othsubo, T. Ishii, J. Nucl. Mater., 125 (1984) 71.

[7]
J. K. Fink, M. G. Chasanov, and L. Leibowitz, "Thermodynamic Properties of Uranium Dioxide" , ANL-CEN-RSD-80-3, Argonne National laboratory, (1981)

[8]
Blackburn, J. Nucl. Mater., 46 (1973) 244.

[9]
J. F. Ready, " Effects of High Power Laser Radiations ", Academic Press (1971).

[10]
Operating Manual for 9300 Series Low Rep Rate Pulsed Laser

Systems, Laser Applications, Inc., Winter Park, FL.

[11]
Photomatic Automatic Pyrometer, Pyrometer Instrument Company, Northvale, NJ

[12]
M. A. Covington, NASA-Ames Research Center, Private Communication (1984)

[13]
S. I. Muzaffar, "Calculation of Surface Temperature Transients of Uranium Dioxide due to Laser Pulsing", M.S. Project Report, Nuclear Engineering Department, University of California, Berkeley (1986)

[14]
M. A. Covington , G. N. Liu, and K. A. Lincoln, " Free-Jet Expansions from Laser Vaporized Planar Surfaces ", AIAA paper no. 76-22 , AIAA 14 th Aerospace Sciences Meeting, Washington, D.C. (1976)

[15]
M. Bober and J. Singer, " High Temperature Vapor Pressure of Metals from Laser Evaporation" , High Temp. Sci., **19** , (1985), 329

[16]
PCR, Incorporated, Gainesville, FL. Technical Bulletin for Product # 18201-4.

[17]
H. Ohashi, S. K. Yagnik, and D. R. Olander, Intl. J. Mass Spectrom. & Ion Proc., **73** , 313 (1986)

[18]
H. U. Karow, " Thermodynamic State and Gas Kinetic Relaxation Behavior of Saturated UO_2 vapor up to 5000 K ", Revue Internationale des Hautes Temperature et des Refractaires, 15 (1978) 347.

[19]
H. U. Karow, " Thermodynamic State, Specific Heat, and Enthalpy of Saturated UO_2 Vapor between 3000 K and 5000 K" , Proc. 7 th Symp. on Thermophysical Properties, national Bureau of Standards, Washington, D.C. (1978).

[20]
R. A. Olstad, "Mass spectrometric Investigation of Laser-Induced vaporization of Binary Solid Compounds", Ph. D. Thesis, University of California, Berkeley, LBL - 1177, (1972)

[21]
W. Breitung, K. O. Reil "In-Pile Vapor Pressure Measurements on UO_2 and $(U,Pu)O_2$ " , KfK 3939, Kernforschungszentrum Karlsruhe, (1985)

[22]
R. Allred, M.S. Thesis, Nuclear Engineering Department, University of California, Berkeley (1987), also D. R. Olander, S. K. Yagnik, R. Allred, to be published.

[23]
E. K. Storms, "Sublimation Thermodynamics of UO_{2-x} " , J. Nucl. Mater., **132** , 231, (1985)

[24]
D. W. Green and L. Leibowitz, "Vapor pressure and Vapor Composition in Equilibrium with Hypostoichiometric Uranium Dioxide at High Temperatures" , J. Nucl. Mater., **105** , 184, (1982)

[25]
C. H. Tsai and D. R. Olander, "The Transition from Free Molecule to Collisional Flow during Vaporization into Vacuum by Test-Particle Method", Phys. Fluids, **30** , (1987) 386.

[26]
S. K. Yagnik, "Condensation Phenomenon in Laser Vaporized Plumes", unpublished work

LAWRENCE BERKELEY LABORATORY
TECHNICAL INFORMATION DEPARTMENT
UNIVERSITY OF CALIFORNIA
BERKELEY, CALIFORNIA 94720